NASA/CR-1998-206948

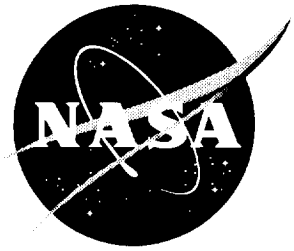

Studies of Shock Wave Interactions With Homogeneous and Isotropic Turbulence

G. Briassulis, J. Agui, C. B. Watkins, and Y. Andreopoulos
The City College of the City University of New York, New York, New York

National Aeronautics and
Space Administration

Langley Research Center
Hampton, Virginia 23681-2199

Prepared for Langley Research Center
under Grant NAG1-1590

March 1998

Available from the following:

NASA Center for AeroSpace Information (CASI)
800 Elkridge Landing Road
Linthicum Heights, MD 21090-2934
(301) 621-0390

National Technical Information Service (NTIS)
5285 Port Royal Road
Springfield, VA 22161-2171
(703) 487-4650

Final Report

NASA GRANT: # NAG-1-1590

STUDIES OF SHOCK WAVE INTERACTIONS WITH HOMOGENEOUS AND ISOTROPIC TURBULENCE

by
G. Briassulis, J. Agui, C. B. Watkins & Y. Andreopoulos
Department of Mechanical Engineering
The City College of the City University of New York
New York, New York 10031

ABSTRACT

A nearly homogeneous nearly isotropic compressible turbulent flow interacting with a normal shock wave has been studied experimentally in a large shock tube facility. Spatial resolution of the order of 8 Kolmogorov viscous length scales was achieved in the measurements of turbulence. A variety of turbulence generating grids provide a wide range of turbulence scales. Integral length scales were found to substantially decrease through the interaction with the shock wave in all investigated cases with flow Mach numbers ranging from 0.3 to 0.7 and shock Mach numbers from 1.2 to 1.6. The outcome of the interaction depends strongly on the state of compressibility of the incoming turbulence. The length scales in the lateral direction are amplified at small Mach numbers and attenuated at large Mach numbers. Even at large Mach numbers amplification of lateral length scales has been observed in the case of fine grids. In addition to the interaction with the shock the present work has documented substantial compressibility effects in the incoming homogeneous and isotropic turbulent flow. The decay of Mach number fluctuations was found to follow a power law similar to that describing the decay of incompressible isotropic turbulence. It was found that the decay coefficient and the decay exponent decrease with increasing Mach number while the virtual origin increases with increasing Mach number. A mechanism possibly responsible for these effects appears to be the inherently low growth rate of compressible shear layers emanating from the cylindrical rods of the grid.

1. INTRODUCTION

The interaction of shock waves with turbulent flows are of great practical importance in engineering applications since they considerably modify the fluid field by vorticity and entropy production and transport. Most of previous work on shock wave/viscous flow interactions is confined in three cases only, namely: Shock wave/boundary layer interaction, shock wave/free shear layer interaction and traveling normal shock/ compressible pipe flow interaction in shock tube.

The present experimental work is a fundamental study of shock wave interactions with nearly homogeneous and nearly isotropic turbulence. A better understanding of the physics involved in this interaction may lead to improvements in turbulence models, which currently are based on incompressible turbulence concepts. The present flow is the best candidate for testing calculation methods and turbulence modeling since all the turbulence kinetic energy which is convected downstream is dissipated locally. There is no new energy production nor, extra strain rates other than that of compression, which may result in additional production or destruction of turbulence. Thus the mean flow field is simplified, and the transport equations are substantially reduced in complexity which makes the modeling issues to play a very dominant role.

The work has focussed on two different, but apparently interconnected, problems: The first one is the interaction of the shock with the flow (see fig. 1a) and the outcome of this interaction and the second problem is the compressibility effects of the incoming flow (see fig. 1b). The major conclusion of this investigation is that the outcome of the interaction depends strongly on the compressibility level of the incoming flow.

a. Shock interactions

In this part of the experimental investigation the effects of shock strength and mesh size of the turbulence generating grid on the flow interactions were addressed independently from each other. Different initial levels of velocity fluctuations and length scales were used before the interaction and their modification after the interaction with a shock wave was studied in detail.

The present work is an extension of the previous work by Honkan and Andreopoulos (1992) and Honkan et al. (1994) and it has been carried out in a shock tube facility with substantially improved spatial and temporal resolution in the measurements of turbulence.

As it was mentioned earlier, previous work on shock wave/viscous flow interactions is confined to three highly anisotropic flow cases : shock wave/boundary layer interaction, shock wave/free shear layer interaction and traveling normal shock/ compressible pipe flow interaction in shock tube.

In the first two cases the shear flow, bounded or free, interacts with an oblique shock generated by a compression corner. In this category, large gradients in static pressure, skin friction and mass flow rate occur and if the turning angle is large enough the flow separates and becomes unsteady due to shock oscillation (Settles, Fitzpatrick and Bogdonoff, 1979: Adamson and Messiter, 1984: Andreopoulos and Muck, 1987: Smits and Muck, 1987: Ardonceau, 1984). Previous work by Hayakawa et al., 1984, Settles et al. (1982), Samimy and Addy (1985) and Samimy et al., (1986) in shock wave/free shear layer interactions indicate similar results as far as the turbulence behavior: considerable amplification of all turbulence intensities across the shock that depends on the shock strength. However, in all previous work on oblique shock wave/shear layer interactions some additional phenomena were involved which made the emerging flow picture and, therefore the flow behavior, rather complicated. These phenomena were: a) oscillation of the shock wave in the longitudinal direction and wrinkles in the spanwise direction; b) separation, occurring downstream of the shock, in cases of a high turning angles which causes even more unsteadiness in the flow field; c) compression continuing after the shock; d) streamline curvature and e) wall proximity which results in high turbulence intensity and, therefore, high flow anisotropy. As a consequence of all these influences, the phenomenon of turbulence amplification as a direct result of the Rankine-Hugoniot jump conditions is considerably distorted and all previous results are masked by these additional effects.

The third category includes flows where turbulence intensities have been considerably amplified after the passage of a shock. This category includes flows inside a shock tube where a traveling normal shock is reflected on the end wall and then interacts with the flow induced by the incident shock (Trolier and Duffy, 1985: Hartung and Duffy, 1986). In these cases turbulence is mainly produced in regions of high velocity gradients close to the wall and then transported towards the center line of the tube. Despite the large scatter of the measured data and the fact that the r.m.s. level of the incident flow was rather low, turbulence amplification was strongly evident. Keller and Merzkirch (1990) measured the density fluctuations in a similar interaction between a traveling wave and a wake of a perforated plate by using speckle photography. They also demonstrated that density fluctuations are considerably amplified. The experimental works, performed in a shock tube, of Honkan and Andreopoulos (1992) and Honkan et al. (1993) mention for the first time the effects on the turbulent scales due to the interaction of the shock wave with grid generated turbulence. Haas and Sturtevant (1987) and Hesselink and Sturtevant (1988), investigated the interaction of a weak shock wave with a single discrete gaseous inhomogeneity and statistical uniform medium respectively. It was found that the shock induced Rayleigh-Taylor instability enhances mixing considerably, in that turbulent scales seem to decrease after passage of the shock. The latter is in contrast to all previous work mentioned earlier and most probably is due to the Rayleigh-Taylor instability which is as a result a non-linear interaction of two pre-existing modes in the flow. Namely that of the vorticity mode and that of the entropy.

The shock wave from a simplistic point of view, can be considered as a steep pressure gradient. Information from experiments and simulation of low speed flows with such pressure gradients indicate that "rapid distortion" concepts hold and, in the limit of extremely sharp gradients the Reynolds stresses and turbulent intensities are "frozen", since there is insufficient residence time in the gradient for the turbulence to alter at all (Hunt, 1973). The physics, associated with the compressibility phenomena that are responsible for this amplification are not well understood.

The first attempt to predict such turbulence amplification is attributed to Ribner (1955). His predictions were verified by Sekundov (1974) and Dosanjh and Weeks (1964).Several analytical and numerical studies of this phenomenon by Morkovin (1960), Zang, Husseini and Bushnell (1982), Anyiwo and Bushnell (1982), Rotman (1991) and Lee et al. (1991, 1993, 1994) show very similar turbulence enhancement. Chu and Kovasznay (1957) indicated that there are three fluctuating modes that are coupled and responsible for the turbulence amplification: 1) acoustic (fluctuating pressure and irrotational velocity mode); 2) turbulence (fluctuating vorticity mode) and 3) entropy (fluctuating temperature mode). These modes are in general, non-linearly coupled and the Rankine-Hugoniot jump conditions across the shock indicate that when any one of the three fluctuating modes is transferred across the shock wave it not only generates the other two but it may also considerably amplify itself. The present work focuses on the turbulence and acoustic (pressure) fluctuation mode. We have

investigated the transfer of homogeneous and isotropic turbulence across an unsteady normal shock propagating inside the flow. Previous work on this subject is rather limited if non-existing. The reason is that is rather difficult to experimentally set-up a configuration where a decaying, grid- generated turbulence will interact with a plane shock in a wind tunnel. Debieve and Lacharme (1985), for instance, attempted to generate homogeneous and isotropic turbulence by installing a grid inside the settling chamber of a supersonic wind tunnel. The flow, however, became anisotropic after it passed through the contraction of the wind tunnel.

One way to simulate experimentally the aforementioned interaction is by taking advantage of the induced flow behind a moving shock in a shock tube. This flow is passed through a turbulence generating grid and the decaying turbulence behind the incident shock interacts with the shock wave after it has been reflected from the end wall.

Previous work in similar flows, as well as on shock wave interactions with boundary layers, indicated that turbulence is drastically amplified through this interaction. Figure 1c shows a typical time-dependent signal of longitudinal vorticity ω_x and longitudinal velocity U during the interaction of a wing-tip vortex with a normal shock of M_s=1.5 .These measurements have obtained by Agui (1998) at City College. Substantial amplifications of velocity fluctuations can be observed after the passage of shock. Amplification of vorticity fluctuations can also be observed.

Furthermore the experiments of Honkan and Andreopoulos (1992) have shown that the amplification of turbulence fluctuations is not the same for different length scales and different turbulence intensities. Direct Numerical Simulations (Lee et al. 1993, 1994) and other theories (see for instance, Anyiwo and Bushnell, 1982) predict this phenomenon. However there is a substantial disagreement between experiments and DNS in predicting the behavior of length scales after the interaction. Integral length scales were found to be reduced by the interaction in experiments as well as in DNS. The dissipation length scales however were found experimentally to increase after the interaction, while DNS indicated a reduction of this scale. It was also found experimentally that amplification of velocity fluctuations is not the same across the entire wave number spectrum. This preferential amplification leads to the increase of dissipation length scales. The linear interaction analysis (LIA) of Ribner (1955, 1986) predicts that the small scales are amplified more than the large scales. Some experimental data from France, provided by Blin (1993) and published in the paper by Jacquin, Blin and Geffroy (1993) indicated no amplification of turbulence. In this case, however, considerable deceleration of the incoming flow before the shock was documented which is known to augment turbulence fluctuations.
The present work is aiming in clarifying several of the issues of disagreement between experiments and theory.

b. Compressibility effects in homogeneous and isotropic turbulence

A fundamental understanding of compressible turbulence in the absence of shock wave interactions, is also necessary for the development of supersonic transport aircraft, combustion processes, as well as high speed rotor flows. Compressibility effects on turbulence are significant when the energy associated with dilatational fluctuations is large or when the mean flow is compressed or expanded. Most of the previous work on compressible turbulence has been carried out in shear layers (see Gutmark et al., 1995, for the most recent review on compressible free shear flows) or boundary layers (see Spina et al., 1994). Previous work on homogeneous and isotropic compressible turbulence (see figure 1b) for a typical flow schematic) is very limited although this flow is the best candidate for testing calculation methods and turbulence modeling. A substantial amount of experimental work dealing with the *incompressible* grid generated turbulence already exists. The effects of grid and perforated plates as flow straighteners on the free stream turbulence was studied by Tan-Atichat et al.(1982) for Reynolds number based on mesh size Re_M up to 735. They found that the performance of the grid is depended on the characteristics of the incoming flow. For larger range of mesh Reynolds number Re_M ranging from 12800 to 81000 Frenkiel et al. (1979) performed experiments where they observed that data exhibit a high degree of similarity. Analysis of the higher order correlations and moments on the turbulent velocity components revealed that the turbulent fluctuations is of non-Gaussian character. Tavoularis et al., (1978) presented a comprehensive study of values of the skewness of velocity derivative for a variety of flow fields and Re_λ. This study indicated that the skewness of the velocity derivative reaches a maximum at Re_λ=5 and then gradually decreases as the turbulent Reynolds number increases.

Grid turbulence at large mesh Reynolds number ($1.2x10^5$ to $2.4x10^6$) was studied by Kistler and Vrebalovich (1966). To avoid compressibility effects the mean flow was kept below 60 m/sec. The flow field under investigation was anisotropic but nevertheless they concluded that if the -5/3 slope is to be used for the spectral curve then a minimum turbulence Reynolds number (Re_λ) of 300 is required. From the literature review it is evident that in all of the above studies on grid generated turbulence compressibility effects were absent or undesirable. One of the first attempts to generate isotropic turbulence is being described by Honkan and Andreopoulos (1992) who set up a flow with $Re_\lambda \approx 1000$. Recently Budwig et al (1995) and Zwart et al. (1996) work with compressible streams for three different Mach numbers in a supersonic wind tunnel. The decay coefficient for the lowest Mach number of 0.16 was found to be -1.24 and for the highest

Mach number of 1.6 was -0.49. Inhomogeneity across the test section prevent them to measure decaying turbulence. The present experimental work is a fundamental study of compressibility effects in grid generated turbulence for flows with Mach numbers ranging from 0.3 to 0.6. The measurements were carried out inside the induced flow behind a traveling shock wave in a shock tube facility. It should be mentioned that in this part of the present work there is no interaction of the flow with the shock wave going through a turbulence generating grid which causes sudden compression of the flow field, as it was in our previous work (Briassulis and Andreopoulos, 1994, 1996).

2. EXPERIMENTAL SET-UP

The experiments were performed in the Shock Tube Research Facility (STURF), shown in figure 2, which is located at the Mechanical Engineering Department of CCNY. The large dimensions of this facility, 1 ft in diameter and 88 ft in length, provide an excellent platform for high spatial resolution measurements of turbulence with long observation time of steady flow. The induced flow behind the traveling shock wave passes through a turbulence generating grid properly installed in the beginning of the working section of the facility. Several turbulence generating grids were used at three different flow Mach numbers. The velocity of the induced flow behind the shock wave, depends on the rupture pressure of the diaphragm, i.e. driver strength. The working (test) section is fitted with several hot-wire and pressure ports. Thus pressure, velocity and temperature data can be acquired simultaneously at various downstream, from the grid, locations of the flow and therefore reduce the variance between measurements. High frequency pressure transducers, hot wire anemometry and Rayleigh scattering techniques for flow visualization have been used in the present investigation.

To assess the flow quality in the facility several tests were carried out. First the shock wave was visualized in order to check its inclination and planform by using a non intrusive optical technique using a YAG laser emitting at the UV range and a UV sensitive, 16 bit CCD camera made by ASTROMED. Second the flow homogeneity was checked by a hot-wire rake constructed for simultaneous acquisition of velocity and temperature data at various radial positions.

To resolve simultaneously two dimensional velocity components with hot wires, a cross wire (X-wire) arrangement was used. New three-wire probes were designed and custom built by AUSPEX Corp. Six different three-wire probe assemblies were used concurrently at different downstream locations, all adjustable to different lengths, each carrying 2 hot-wires in an X configuration and one cold-wire for simultaneous velocity and temperature measurements respectively. The three-wire probes were equipped with 5 μm Platinum/Tungsten wires for velocity measurements and with a 2.5 μm Platinum/Tungsten wire for temperature measurements. To eliminate any wake effects from upstream probes on any downstream, all of the probes were staggered at different distances from the tube wall and 90 degrees apart every other probe. Figure 3 shows the above arrangement of the X-wire probes and their downstream from the grid location. The cross wires were driven by DANTEC anemometers model CTA56C01 and the temperature wires were connected to EG&G model 113 low noise, battery operated pre-amplifiers/filters. For more details on the hot-wire techniques applicable to shock tubes see Briassulis et al. (1995) where estimates of uncertainties in the measurements are also given.

In order to measure space-time correlations a rake with five hot-wire probes was designed and constructed. The probes of the rake carrying a 5 μm Platinum/Tungsten wire (hot-wire) and a 2.5 μm Platinum/Tungsten wire (cold-wire), were equally spaced 2 inches apart and permanently attached on the rake's tube. The rake assembly was placed at a hot-wire tap 24 in. downstream from the grid as shown in figure 4.

Time dependent pressure fluctuations were obtained by several miniature high frequency Kulite pressure transducers, type XCQ-062, installed on the shock tube wall.

During the different sets of experiments all of the signals were acquired simultaneously with the ADTEK data acquisition system. The ADTEK AD830 board is a 12 bit EISA data acquisition system, capable of sampling simultaneously 8 channels at 333 KHz each channel. Three of those boards are currently available providing 24 simultaneous sampled channels at 333 KHz per channel. It should be mentioned that no sample-and-hold units were used in the present data acquisition since each channel was dedicated to an individual Analog to Digital converter.

The experimental set-up provided time dependent measurements of two velocity components, temperature and wall pressure at several locations of the flow field simultaneously.

The bulk flow parameters of the experiments performed are summarized in table I and include the grid size m, the mesh size M, the flow Mach number M_{flow}, the mesh Reynolds number Re_M and the turbulent Reynolds number $Re\lambda$..

3. ISOTROPIC DECAY RELATIONS

Three characteristic regions can be found in the flow behind a grid. First is the developing region close to the grid where rod wakes are merging and production of turbulent kinetic energy takes place. This region is followed by one where the flow is nearly homogeneous and isotropic but where appreciable energy transfer from one wave number to another occurs. This region is best described by the power law decay of velocity fluctuations

$$\frac{\overline{u^2}}{\overline{U^2}} = A\left[\frac{x}{M} - \left(\frac{x}{M}\right)_0\right]^{-n} \qquad (1)$$

where A is the decay coefficient, $(x/M)_0$ is the virtual origin, n is the decay exponent.
The third region or final region of decay is the farthest downstream of the grid and is dominated by strong viscous effects acting directly on the large energy containing eddies.

Compressible homogeneous and isotropic turbulence has not been yet set-up experimentally and decay laws for this case have yet to be established. The turbulent or fluctuation Mach number $M_t = \frac{q}{c}$ seems to be the most appropriate parameter describing compressible turbulence. By extrapolating the validity of the previous law into compressible flows one can obtain the power law decay

$$M_t^2 = B\left[\frac{x}{M} - \left(\frac{x}{M}\right)_0\right]^{-n} \qquad (2)$$

where $B = 3A\,M_{flow}^2$ and B, $(x/M)_0$ and n depend on the grid size, mesh Reynolds number (Re_M) as well as the mean flow Mach number M_{flow}.

The turbulent kinetic energy transport equation is (Lee et al, 1993)

$$\bar{\rho}\tilde{u}_k\frac{\partial\overline{(u_iu_i/2)}}{\partial x_k} + \bar{\rho}R_{ik}\frac{\partial\tilde{u}_i}{\partial x_k} + \bar{u}_i\frac{\partial\bar{P}}{\partial x_i} + u_i\overline{\frac{\partial p}{\partial x_i}} + \frac{\partial\overline{(\rho u_iu_iu_k/2)}}{\partial x_k} - u_i\overline{\frac{\partial\tau_{ik}}{\partial x_k}} = 0$$

where R_{ij} is the Reynolds stress tensor defined as: $R_{ij} = \overline{\rho u_i u_j}/\bar{\rho}$ where $\tilde{u}_k$ is the mass-weighted average and u_k is the fluctuation from $\tilde{u}_k$ according to Favre (1965).

In any part of the flow, production by the mean strain is zero as well as work by mean pressure. Work done by pressure fluctuations and turbulent transport have been found by Lee et al. to be very small. Therefore for the present case of homogeneous turbulence

$$\bar{\rho}\tilde{u}_k\frac{\partial q^2/2}{\partial x_k} = u_i\overline{\frac{\partial\tau_{ik}}{\partial x_k}}$$

$$-\tilde{u}_k\frac{\partial q^2/2}{\partial x_k} = -\frac{1}{\bar{\rho}}u_i\overline{\frac{\partial\tau_{ik}}{\partial x_k}} = \varepsilon \qquad (3)$$

where $q^2 = \overline{u_iu_i}$.

Thus measurement of the convection of $q^2/2$ by the mean flow can provide a good estimate of the dissipative viscous term ε and its length scale L_e through

$$-\overline{U}\frac{\partial\overline{q^2}}{\partial x} = \varepsilon = \frac{\left(\overline{q^2}\right)^{\frac{3}{2}}}{L_e} \qquad (4)$$

Once the calculation of the previous dissipation length scales is obtained then the dissipation rate ε as well as the associated micro scales (length, time, velocity) can be calculated. The above equation can be transformed to the following relation by non dimensionalizing with the mesh size M:

$$-\frac{\varepsilon M}{\overline{U}^3} = \frac{3}{2}\frac{\partial\left(\overline{u^2}/\overline{U}^2\right)}{\partial(x/M)} = \frac{3}{2}\frac{\left(\overline{u^2}\right)^{\frac{3}{2}}}{L_e}\left[\frac{M}{\overline{U}^3}\right] \qquad (5)$$

From equation (5) the decay rate can be calculated using the coefficients of the power law of equation (1). Substitution of (1) in equation (5) yields:

$$\varepsilon = \frac{3}{2}nA\left[\frac{x}{M} - \left(\frac{x}{M}\right)_0\right]^{(-n-1)}\left[\frac{\overline{U^3}}{M}\right] \qquad (6)$$

where A is the decay coefficient, $(x/M)_0$ is the virtual origin, n is the decay exponent, U is the mean flow velocity and M the mesh size.

4. ESTIMATES OF DISSIPATION RATE OF TURBULENT KINETIC ENERGY

The dissipation rate of turbulent kinetic energy ϵ is defined as $\epsilon = 2\nu S_{ij}S_{ij}$ where S_{ij} is the strain-rate-tensor. Direct evaluation of ϵ is very difficult to carry out because it requires simultaneous, highly resolved measurements of nine velocity gradients at a given location of the flow field. Fortunately, for isotropic turbulent flows with moderate or low Mach number fluctuations, the above relation is considerably simplified to $\epsilon = 15\nu\overline{\left(\frac{\partial u}{\partial x}\right)^2}$ (Tennekes and Lumley, 1972). In the present case the dissipation rate ϵ has been computed by four different methods:

1. From the decay rate of turbulent kinetic energy and the use of equations 5 and 6.
2. From frequency spectra of velocity fluctuations after invoking Taylor's hypothesis to compute the three dimensional wave number spectrum E(k). The dissipation ϵ can be computed from the integral .

$$\epsilon \approx 2\nu\int_0^\infty k^2E(k)dk$$

3. From estimates of $\overline{\left(\frac{\partial u}{\partial x}\right)^2}$ and the isotropic relation $\epsilon = 15\nu\overline{\left(\frac{\partial u}{\partial x}\right)^2}$. The quantity $\overline{\left(\frac{\partial u}{\partial x}\right)^2}$ has been computed by differentiating in time the velocity fluctuation signal and invoking Taylor's hypothesis of frozen turbulence convection.
4. From estimates of Taylor's microscale λ obtained from autocorrelations of longitudinal velocity fluctuations. Then the rms of the fluctuations of the velocity gradient $\overline{\left(\frac{\partial u}{\partial x}\right)^2}$ can be obtained independently from $\overline{\left(\frac{\partial u}{\partial x}\right)^2} = \frac{u^2}{\lambda^2}$ and therefore dissipation can be computed from $\epsilon = 15\nu\frac{u^2}{\lambda^2}$.

The estimates usually obtained from these methods are not identical since the uncertainties involved in each of them may

differ considerably. The lack of adequate spatial resolution is one of the major source of errors and affects each estimate of ϵ differently. However even in cases where the estimates of ϵ differ by 50% or more the estimates of L_e or Kolmogorov's viscous scale $\eta \equiv \left(\frac{\nu^3}{\epsilon}\right)^{\frac{1}{4}}$ differ only by 8.5% (see Honkan and Andreopoulos, 1997). In the present case the estimates of ϵ obtained from the decay rate of q^2 and those obtained from Taylor's microscale (autocorrelations) were the most reliable. Based on these estimates of ϵ the spatial resolution of probe used in the present investigation was between 7 η and 26 η, depending on the operating conditions of the flow. If one considers that the spatial resolution usually achieved in measurements of compressible flows is of the order of $10^3\eta$ (see Andreopoulos and Muck, 1985; Smits and Muck, 1984) then the present one appears to be very satisfactory even if it is compared to that usually achieved in low Reynolds number incompressible flows.

5. FLOW HOMOGENEITY AND ISOTROPY

Figure 5 shows a snapshot image of the shock wave and the induced flow behind it. It was visualized by introducing liquid N_2 in the flow to increase the scattered light, since the elastic scattering of UV light of the air molecules of the flow was rather weak for the present density changes. As opposed to supersonic wind tunnels where the low temperature environment causes substantial condensation of water vapors which subsequently introduces adequate light scatterers for flow visualization, the high temperature of the flow in shock tubes precludes the use of the same materials for stronger light scattering. The flow visualization experiments and quantitative analysis of velocity and temperature across a section of the tube indicated that the flow is homogeneous within 85% of the diameter.

The flow isotropy was verified directly and indirectly. Direct verification provided by computing the anisotropy tensor b_{ij}.

$$b_{ij} = \frac{\overline{u_i u_j}}{\overline{u_i u_i}} - \frac{1}{3}\delta_{ij} \qquad (7)$$

where u is velocity fluctuation about the mean and δ_{ij} is the Kronecker delta.

The present data suggest a rather low degree of anisotropy which although not perfect is within well established margins. For comparison it should be mentioned that for boundary layers b_{11}=0.45 and b_{12}=0.15. The anisotropic tensor b_{ij}, shown in figure 6, established the isotropic nature of the flow. Anisotropy of the present flow field is compared with one of the latest and most complete studies in this matter of Tsinober et al. (1992) in incompressible flows.

Indirect evidence of isotropy was provided by considering the skewness of velocity fluctuations and the skewness of velocity derivative (Tavoularis et al., 1978, Mohamed and LaRue, 1990).

Figure 7 presents the skewness of velocity fluctuations for three mean flow Mach numbers. It appears that S_u remains constant and close to zero for all measured downstream locations. The skewness of velocity derivative has been found experimentally to depend on the turbulent Reynolds number, Re_λ. Tavoularis et al., (1978) presented a comprehensive study of values of the skewness of velocity derivative for a variety of flow fields and Re_λ. From this study, if one considers the data obtained from isotropic grid turbulence, it can be observed that $S_{\partial u/\partial x}$ decreases for Re_λ>5. Typical values for $S_{\partial u/\partial x}$ are shown for three different flow cases in figure 8 together with values obtained from various turbulent flow fields. The values obtained are between 0.2 and 0.4 , a range which is lower than the $S_{\partial u/\partial x}$ value at $Re_\lambda \simeq 5$. Determination and calculation of the skewness of velocity derivative requires additional consideration. It is described in detail in the Thesis by Briassulis (1995).

It can be therefore concluded from all these direct and indirect evidence that the present flow is nearly homogeneous and isotropic.

6. DECAY OF MACH NUMBER FLUCTUATIONS

Several grids were used in the present experiments so the Reynolds number based on the mesh size Re_M as well as the dominant length scales present in the flow can be varied. The mesh Reynolds number was ranging from 35,000 to

600,000 while the mesh size was ranging from 3mm to 25mm. Measurements were obtained at three different driver pressures/shock strengths. The bulk parameters of all flow cases are shown in table 1.

The typical decaying with x/M of turbulent kinetic energy data was fitted with the power law of equation (1). In this fitting the variables A, $(x/M)_0$, and n were determined so that the residual deviation from the original data to be minimal. The present work documents the effects of the mesh size/mesh Reynolds number as well as the flow Mach number on the above mentioned variables. The importance of this parameters is evident when one studies eq (6). The dissipation rate ε can be computed once those parameters are known. This provides an alternate method of calculating ε.

Figure 9 demonstrates the power law decay behavior of all the measured data as it is described by equation (2). The results of 6 experiments are plotted in logarithmic scales in this figure. They include 3 different grids at three different pressures/mean flow Mach numbers. Several conclusions can be drawn from their data. First the exponent n and the constant B depend on the grid, Mach number or Re_M and second that the region where isotropy starts, depends more on the grid than on the flow Mach number or Re_M.

The effect of Re_M/M and Mach number on the coefficient A is shown in figure 10. Reynolds number variation was produced by changing the mesh size under a constant velocity.

For the lowest tested velocity flow field ($U \simeq 120$ m/sec), which corresponds to a mean flow Mach number of 0.35, the decay coefficient A increases in a non-linear fashion with increasing mesh size M as shown in figure 10. As the Mach number increases, A is substantially decreased from the previous case and furthermore it appears to be independent of mesh size. The same holds for the highest tested Mach number, where the decay coefficient is further suppressed. It can be concluded that the decay coefficient A decreases when the Mach number increases.

The virtual origin $(x/M)_0$ strongly depends on the mesh size/Re_M. For all cases it was observed that the virtual origin approaches the grid as the mesh size/Re_M increases as shown in figure 11, most probably due to increased mixing which is associated with increasing Re_M. The effects of the Mach number can be seen in figure 12. The virtual origin is mainly affected at the highest Mach number only, while for the medium and low cases remain unaffected. At the highest Mach number and the associated compressibility effects the virtual origin moved further away from the grid. It is interesting to observe, in the same figure, that the above mentioned effect is diminished for the largest mesh size. Namely the virtual origin at high Re_M appears to reach the same value about 5 mesh sizes for all the investigated Mach numbers.

The decay exponent n, shown in figure 13, is substantially affected by the Mach number of the flow field. It is clear from the above figure that n is decreasing with increasing Mach number. The effect of the mesh size on the decay exponent can also be observed. It behaves similarly to the decay coefficient A. Namely for the lowest Mach number it increases with increasing mesh size/Re_M. That means that for finer grids, i.e of small mesh size, there exists larger decay rates than for coarser grids. At a first glance the above statement appears to contradict previous notions based on fixed n fitting of the data, but if we consider equation (6) then the dissipation rate ε is inversely proportional to $\{nA(x/M-(x/M)_0)^{(n+1)}$. Thus ε will increase if n decreases.

When the Mach number increases the opposite trend can be seen. The decay exponent is decreasing with increasing mesh size for the medium shock strength and it remains more or less constant for the highest shock strength at $n \simeq 0.3$.

A typical decay of velocity fluctuations, as fitted by the power law, for a 5.08 mm mesh size is shown in figure 14. The velocity fluctuations are higher at higher Mach numbers and Re_M. The effect of higher velocity fluctuations can not simply be attributed to the increase of the mean Mach number and the associated compressibility effects of the flow but also to the increase of Re_M. A 4-fold increase in pressure which corresponds to 100% change in Mach number and Reynolds number results in a 3 fold increase in the Mach number fluctuations M_t, throughout the entire flowfield. Most probably this increase in M_t and $(u/U)^2$ can be attributed to both parameters, i.e. M_{flow} and Re_M.

7. DISSIPATION RATE AND LENGTH SCALES

Figure 15 shows the dissipation rate of kinetic energy ε for one grid at different flow Mach numbers. It appears that ε as well as the kinetic energy, increases with increasing Mach number in all investigated subsonic flows. It remains to be seen whether this effect is a Mach number effect or it is due to Reynolds number increase.

The dissipation rate of kinetic energy ϵ for various mesh sizes is shown in fig. 16 at the highest tested Mach number flowfield. For the highest Mach number the coarser grid and higher Re_M did not produce higher dissipation rates as was implied from figure 15. In this figure the effects of Re_M/M at a fixed flow Mach number, M_{flow} can be depicted. Namely, figure 16 suggests that coarser grids, i.e. higher Re_M produce lower dissipation rates, ϵ, when compressibility effects are high. In the absence of large compressibility effects, which are typical in the lowest tested Mach number flowfields, the

reverse influence of the mesh size on ϵ non-dimensionalized by the mean velocity and mesh size has been found as is shown in figure 17. In this figure, non-dimensionalized ϵ for the lowest tested flowfield of M_{flow}=0.35 is plotted for various mesh sizes. The reverse trend is observed for $\epsilon M/U^3$ in the absence of strong compressibility effects. Since the mean flowfield velocity U is equal for all plotted cases the effect presented in this figure is mainly due to the Mesh size M and Re_M. In this case, the coarser grid with the largest mesh size and highest Re_M shows the largest non dimensionalized dissipation rate of kinetic energy. For even higher mean Mach number flowfields (see figure 18) the effect of compressibility is rather striking where, once more, the opposite trend of the dependence of $\epsilon M/U^3$ to the mesh size/ Re_M is shown. For the medium tested Mach number flowfield case the effect of the grid's mesh size becomes obvious when figure 19 is studied. From this figure it can be summarized, that the coarser grids with the greater mesh sizes and highest Re_M flowfield produce a lower dissipation rate ϵ. The dissipation rate of kinetic energy for the medium tested Mach number follows the trend that exists for the highest tested Mach number and therefore suggest that the presence of compressibility effects are felt in this flowfield too. The difference and the influence of the compressibility effects for both flowfields can be estimated upon closer investigation of figures 16 and 19. For almost a 4-fold increase in the mesh size and Re_M the dissipation rate decreased 10 times for M_{flow}=0.6 and approximately 5 times for the M_{flow}=0.475 flowfield. This verifies that higher Mach number flowfields introduce higher compressibility effects.

The dissipative length scale L_e indicates how fast the advected turbulent kinetic energy q^2 at a given location, is dissipated in to heat. As Mach number increases the results of the present investigation show that the dissipative length scale L_e increases although the dissipation rate of turbulent kinetic energy, ϵ, also increases. This increase in L_e is attributed to the increase in q^2 with Mach number which apparently is larger than the corresponding increase of ϵ.

A typical result is shown in figure 20 for the flow at three different Mach numbers and for the same mesh size. It is interesting to observe that for the highest mean flow Mach number the dissipation length scale increased much more than for the medium case. Higher compressibility effects and higher Re_M are the only logical parameters than can cause such a drastic increase. The effect of the grid's mesh size on the dissipation length scale is shown in figure 21. The dissipation length scale L_e increases with increasing mesh size and Re_M. From this figure it can be seen that for the same mean Mach number a 5-fold increase in L_e occurs for a 3-fold increase in the mesh size/Re_M. The pivotal effect that the grid size exerts on the length scales in the flowfield should be clear by now. It is apparent from both previous figures that the dissipation length scale strongly depends on x/M.

The effect of Mach number on the Taylor's microscale computed from $\epsilon = 15\nu\overline{\left(\frac{\partial u}{\partial x}\right)^2} = 15\nu\frac{u^2}{\lambda^2}$ is shown in figure 22 for three different Mach numbers and for the same mesh size. The Taylor's microscale appears to increase with increasing Mach number. Increase of the Taylor's microscale is also observed for the flowfield produced by coarser grids. This is shown in figure 23 where four different grid sizes at the same Mach number are plotted. It is clear that the coarser the grid, larger mesh size, the greater the Taylor's microscale. The dependance (increase) with increasing x/M is evident, as shown earlier for the dissipation length scale, is also shown for the Taylor's microscale.

As the Mach number increases the Kolmogorov's length scale (η) decreases as it can be seen in figure 24 for M=5.08 mm. This result was expected since the dissipation rate of kinetic energy increases with increasing Mach number. Thus from the definition of $\eta = \left(\frac{\nu^3}{\epsilon}\right)^{\frac{1}{4}}$ the previous result was obtained.

The effect of the different mesh sizes on the viscous scales can be shown for a constant velocity flowfield but with different mesh size turbulence generating grids. Experimental results showed that the Kolmogorov's length scale increases as the mesh size increases. Figure 25 presents four different mesh sizes for a decaying flowfield at a constant mean Mach number of 0.6. Similar results are obtained for the rest of the tested flowfields.

The last two figures (24 and 25) can verify the influence of the compressibility effects on the viscous scales. Since η increases as the mesh size and Re_M increase, then one might expect figure 25 to show an increase of η when Re_M is increased by increasing the velocity of the flowfield only (mean flow Mach number). The latter trend is shown in figure 24 to be incorrect and rather high compressibility effects associated with the corresponding flowfields are credited for such behavior of η. Namely for the case of the viscous scales, compressibility effects appear to suppress their size. The above mentioned measurements indicate values of η ranging from 0.015 to 0.06 mm. The size of the probes expressed in terms of Kolmogorov's length scales appears to be $\eta_w = l_w/\eta = 13$ for the greatest scales and 52 for the smallest scales. The scales at error start at about half of these values, 7 and 26 respectively. Based on these values, which determine the upper limit of the valid part of the spectrum, estimates of the spectral power density of the spatially filtered scales have been obtained from Wyngaard's (1968) work for subsonic flows. It appears that the spatially filtered scales amount to about 15% of the

total spectral density of velocity fluctuations for measurements close to the grid where η is small and less than 4% for measurements where η is larger. The high resolution of the hot wire probes allows us to conclude that the results obtained in regard to the compressibility effects on the viscous scales are not biased.

8. THE INTERACTION OF DECAYING TURBULENCE

Figure 26a shows the decay of the Mach number fluctuations downstream of the 2x2 (2 meshes per inch) grid before the interaction. It can be seen that the experimental data obey very closely the power law decay described by equation 2. It also clear that M_t increases with the mean flow Mach number M i.e. driver pressure as shown earlier. After the passage of the shock the flow field changes. Velocity fluctuations in the longitudinal direction increase and Mach number fluctuations (shown in figure 26b) are changed also but not very drastically because the amplification of velocity fluctuations u is offset by an increase in mean temperature due to the compression. Thus M_t after the interaction sometimes is higher and sometimes is lower than before the interaction.

Figure 27a demonstrates the power law decay behavior of all the measured data as it is described by equation (2). The results of 6 experiments are plotted in logarithmic scales in this figure. They include 3 different grids at three different pressures/mean flow Mach numbers and they correspond to the data shown in fig. 9.

The results after the passage of the shock are shown in figure 27b. The large region of a linear behavior in this log-log plot indicates that the flow follows the same power law decay with different n, B and $(x/M)_0$. This is an indication that there is a quick return to isotropy of the flow after the passage of the shock which can be considered as a strong axisymmetric disturbance imposed on the isotropic field.

Determination of the virtual origin $(x/M)_0$, decay exponent n and decay coefficient B was accomplished by fitting the experimental data to the power law of equation (2) so that the standard mean square deviation is minimized (see Mohamed and LaRue, 1990). Figure 28 shows a typical variation of the decay exponent n before and after the interaction with the shock wave of $M_s \approx 1.37$ for various mesh sizes of grids. The results show that n is a function of the mesh size i.e. initial conditions before the interaction and that these values are substantially less than one. The effect of the shock interaction is very dramatic and depends on the M_s, M_{flow} and initial conditions.

Figure 29 presents the ratio of the decay coefficient, after the interaction with the shock to that before the interaction, n_d/n_u. It can be seen that this ratio is always greater than one for all investigated cases. In the lowest subsonic flow interaction with a $M_s \approx 1.2$ shock, this ratio appears independent of initial conditions. This is in agreement with Mohamed and LaRue, 1990. In the case of $M_{flow}=0.475$ this ratio is very high at small Re_M and decreases to 1.25 at high Re_M where it remains independent of it. At higher Mach numbers this ratio increases dramatically with Re_M. Thus n_d/n_u depends on initial conditions, flow Mach number M_{flow} and shock strength M_s.

It was shown previously in section 6 that the velocity fluctuations are higher for higher mean Mach number flowfields. The opposite trend is evident after interaction in figure 30 where the flowfield is compressed by the reflected shock wave. Namely, after the interaction of the flow with the reflected shock wave, the lower Mach number flow possesses the higher velocity fluctuations. Similar results are observed for the other coarser grids (larger mesh sizes). The effect of the grid size on velocity fluctuations can be verified from figures 30 and 31. It appears that there exists higher velocity fluctuations in flowfields produced by finer grids with lower Re_M.

From the information on the decay of velocity fluctuations and the use of the power law, the dissipation of kinetic energy for the compressed by the shock wave flowfield can be obtained by:

$$\epsilon = \frac{3}{2} nA \left[\frac{x}{M} - \left(\frac{x}{M} \right)_0 \right]^{(-n-1)} \left[\frac{\overline{U_u^2 U_d}}{M} \right]$$

where the subscripts u and d refer to the mean flow upstream and downstream of the shock wave respectively. In general it can be concluded that the dissipation rate of kinetic energy (ϵ) is drastically decreased after the interaction of the flowfield with the reflected shock wave. Typical results of ϵ are shown in Figures 32 and 33 for two different grids at the highest Mach number tested.

From the analysis of the dissipation rate of kinetic energy the dissipative length scale, L_ϵ, can be calculated

as $-\bar{U}\frac{\partial \overline{q^2}}{\partial x} = \epsilon = \frac{(\overline{q^2})^{\frac{3}{2}}}{L_e}$. In general, experiments have shown that the dissipative length scale increases after the flow has been compressed by reflected shock wave as seen in figure 34 and depends on x/M. As turbulence decays with larger x/M, the dissipative length scale (L_ϵ) increases substantially. It is also shown that at larger x/M, where the length scales have grown to larger sizes the dissipative length scale was amplified the most.

The effect of the mesh size as well as the effect of the sudden compression of the flowfield by the reflected shock wave on the Taylor's microscale (λ) are the principal parameters in such type of flows. In all cases the Taylor's microscale, obtained by $\epsilon = 15\nu\overline{\left(\frac{\partial u}{\partial x}\right)^2} = 15\nu\frac{u^2}{\lambda^2}$, increases due to the compression of the flow by the reflected shock as shown in figure 35. It is obvious that λ depends on x/M and this amplification is greater at larger x/M where the microscale has grown. As observed in the decaying flowfield the grid is the principal control parameter of the length scales present in the flowfield. The effect of the grid's mesh size on the Taylor's microscale for the flowfield compressed by the shock wave is shown in figure 36 for several grids and the same mean Mach number flowfields. The figure shows the coarser grids to introduce larger scales than the finer grids. The dependance of λ on x/M is clearly shown in the above mentioned figure.

The hot wire probes that were used were able to resolve 7-26 Kolmogorov's length scales. Previous experiments (Andreopoulos and Muck, 1987, and Smits and Muck, 1987) report resolutions of 300-1000 viscous length scales. Even though the present resolution is not ideal, physical constraints on the construction and operation of the probes do not allow us to achieve a better resolution. Nevertheless the current resolution achieved is the highest reported for such type of flow measurements. Resolution of 7-26 Kolmogorov's length scales yielded an excellent understanding of the bulk characteristics of the behavior of such scales. The Kolmogorov's length scale (η) defined as $\eta \equiv \left(\frac{\nu^3}{\epsilon}\right)^{\frac{1}{4}}$, increases after the flowfield has been compressed by the reflected shock wave. This is shown in figure 37 where it is clear that η increases as x/M increases (i.e. as turbulence decays and length scales grow).

9. SPACE-TIME CORRELATIONS AND LENGTH SCALES

In order to estimate the length scales in the longitudinal ξ_1 direction and normal ξ_2 the cross correlation coefficients

$$r_{ij}(\xi_k) = \frac{\overline{u_i(x)u_j(x+\xi_k)}}{\sqrt{\overline{u_i^2(x)}}\sqrt{\overline{u_j^2(x+\xi_k)}}}$$

were evaluated by two point measurement in the ξ_2 direction and from auto-correlations in the ξ_1 direction after invoking Taylor's hypothesis.

Figure 38 shows the $L_{11}(\xi_1)$ in the longitudinal direction before the interaction for the three different flow cases before the interaction with the shock wave. There exists some scatter in the data in each particular case which is attributed to the various grids used. It can be seen that the integral length scale increases with downstream non-dimensional distance x/M for all investigated cases. It is also evident that L_{11} in the case of M_{flow} =0.475 is higher than in the case of M_{flow} =0.36. However when the flow Mach number increases to M_{flow} =0.6 and therefore stronger compressibility effects are present, then the integral length scale drops.

After the interaction with the shock wave the distribution of $L_{11}(\xi_1)$ is more complicated (see fig. 39). All the scales are reduced considerably. However the reduction of the larger scales is greater. This is also shown in figure 40 where the attenuation ratio

$$G_{L_{11}} = \frac{L_{11,d}(\xi_1)}{L_{11,u}(\xi_1)}$$

is plotted. At large x/M where the initial scales were the largest the reduction is dramatic. Thus once again it is found that amplification or attenuation is not the same for all initial length and velocity scales. It is interesting to observe that the stronger the shock strength the greatest the attenuation of the longitudinal length scales.

The two point correlation $r_{11}(\xi_2)$ in the lateral direction ξ_2 of the longitudinal velocity fluctuations is shown in figure 41. These data were obtained by a specially designed cross correlation probe of six parallel wires and three temperature wires separated from each other by 1mm. Not all the curves cross the zero line and therefore it is very difficult to integrate them in order to obtain the classically defined length scale in the lateral direction. However the slopes of these curves are indicative of their trend. It is rather obvious that the length scales before interaction are reduced with increasing flow Mach number. This behavior is very similar to that of $L_{11}(\xi_1)$. After the interaction, however the length scale $L_{11}(\xi_2)$ increases in the first two cases and decreases in the strongest interaction.

In order to investigate the effect of initial conditions on this correlation at the highest flow and shock Mach number where the lateral scales are shown to reduce (fig. 41) various grids were used. The data shown in figure 42 indicate that the correlation increases substantially in the case of the finest grid, 8x8 with the lowest Re_λ, after the interaction. However the coarser grid, 2x2 grid with the highest Re_λ=737, shows the greatest attenuation in the lateral integral scale of turbulence after the interaction.

The effect of the shock strength on the velocity fluctuations is shown in fig. 43. For the 1x1 grid, it appears that the amplification of turbulence fluctuations defined as

$$G_u = \frac{u_{rms,d}}{u_{rms,u}}$$

increases with downstream distance for a given flow case and interaction. As the M_{flow} increases G_u also increases. For finer grids the effects of shock interaction are felt differently. For the 2x2 grid for instance, the data show that in the first case of a practically incompressible upstream flow interacting with a rather weak shock, amplification of turbulence occurs at x/M>35. The amplification is greater when M_{flow} increases to 0.436. However, when compressibility effects in the upstream flow start to become important no amplification takes place (G_u is about 1).

Some more dramatic effects of compressibility are illustrated in figure 44, where the amplification G_u is plotted for the case of a finer grid with mesh size 5x5. The interaction of a weak shock with a practically incompressible turbulent flow produces the highest amplification of velocity fluctuations with G_u reaching a value close to 2. As the M_{flow} increases, G_u decreases and at M_{flow} = 0.576 a slight attenuation occurs at downstream distances. It is therefore plausible to conclude that for high shock strength (high Mach number) compressibility effects control the velocity fluctuations which are generated by fine grids and no amplification of turbulent kinetic energy is observed.

Hannapel and Friedrich (1995) have also shown in their DNS work that compressibility effects in the upstream reduce turbulence amplification significantly. The Linear Interaction Analysis of Ribner, which was initially developed for an incompressible isotropic turbulent field, predicts amplification of turbulence fluctuations. Mahesh, Lele and Moin (1997) have shown recently that LIA as well as DNS may show a complete suppression of amplification of kinetic energy if the upstream correlation between velocity and temperature fluctuations is positive. It is therefore possible that in case of very fine grids and high Mach number flows where the dissipation rate of turbulent kinetic energy is high (see figures 15 and 16) that entropy fluctuations may be responsible for completely suppressing turbulence amplification.

Rapid Distortion Theory (see Jacquin et al., 1993) also shows substantial damping of amplification due to pressure fluctuations. Our pressure fluctuation data at the wall beneath the boundary layer show significantly higher amplification of pressure fluctuations G_p (see figure 50) for finer grids. If the damping effects of pressure were ignored RDT leads to the following simple relation for G_u

$$G_u = \left[\frac{(2+C^2)}{3}\right]^{1/2}$$

where $C=\rho_d/\rho_u$. In the present experiments C is between 1.25 to 1.7 which indicates that G_u is between 1.09 to 1.3 .

Although the decay exponent increases after the interaction (see also Jacquin, 1991), the dissipation rate of kinetic energy decreases because ϵ is proportional to:

$$An\left(\left(\frac{x}{M}\right)-\left(\frac{x}{M}\right)_0\right)^{-n-1}$$

Attenuation of the dissipation rate of kinetic energy is of the order of 0.3 for all the grids tested at the highest Mach

number. A 3-fold decrease of the dissipation rate of kinetic energy is found for the interacted (compressed) flow as shown in figure 45. It is interesting to observe that at this high mean Mach number which produced flowfields with the greatest compressibility effects, the grid's mesh size appears to be inconsequential to the attenuation of the dissipation rate of kinetic energy.

The effect of the shock strength / mean flow Mach number on the attenuation of the dissipation rate was found when the mesh size was kept constant and data presented for experiments of different mean flow Mach numbers is shown in figure 46. It is clear that the higher the mean flow Mach number/compressibility effects, the greater the attenuation of the dissipation rate of kinetic energy. A 3-fold attenuation of ϵ is observed for high (M_{flow}=0.7) and medium (M_{flow}=0.5) shock strengths and a 2-fold attenuation for the lowest case (M_{flow}=0.3). The attenuation of ϵ after the interaction of the flowfield with the reflected shock wave was also independently calculated by integrating the wavenumber spectrum before and after the interaction. The ratio of the two integrals is shown in the same figure (scattered points). It is clear that both methods present the attenuation of the dissipation rate of kinetic energy after interaction with the shock wave.

The dissipative length scales L_e, which express the distance within which the advected turbulent kinetic energy is directly dissipated, increase after the interaction with the shock because the dissipation rate is attenuated.

Figure 47 shows the amplification of the dissipative length scales defined as:

$$G_L = \frac{L_{e,d}}{L_{e,u}}$$

where $L_{e,d}$ and $L_{e,u}$ are the length scales downstream and upstream of the shock respectively. At each location x/M, L_e and turbulence intensity are different. The results suggest that at large x/M where L_e is indeed large and velocity fluctuations are small, L_e is amplified more. The data also indicate that G_{Le} is increased with shock strength.

The present high resolution measurements, with hot-wire length of the order of 8 or less viscous units, allowed for analysis of the data of the viscous scale level. Most of the previous experiments of compressible turbulence were carried out with resolution of 300 to 1000 viscous length scales. Figure 48 shows the amplification of the viscous scales defined as:

$$G_\eta = \frac{\eta_d}{\eta_u}$$

where $\eta = \left(\frac{\nu^3}{\epsilon} \right)^{\frac{1}{4}}$.

It is interesting to observe that G_η is considerably smaller than G_{Le} and that it behaves somehow differently. G_η decreases with downstream distance and shock strength. The different behavior of G_{L11}, G_{Le} and G_η clearly suggest that the result of the shock interaction is not felt uniformly across all the length scales of the flow: Larger eddies are amplified or attenuated more than smaller eddies. Both length scales L_e and η depend on the dissipation rate ϵ which in all experiments has been found to be reduced after the interaction to about 0.2 of the upstream value. The DNS of Lee et al. (1993) indicate a moderate increase in ϵ after the shock interaction. This difference between the present experimental results and those of DNS leads to different, qualitatively, description of the effect of the shock interaction on length scale. In order to further assess the behavior of length scale independently from ϵ, the Taylor's microscale $\lambda_x = \left[\frac{\overline{u^2}}{\left(\frac{\partial u}{\partial x} \right)^2} \right]^{\frac{1}{2}}$ has been computed from the time derivative of u velocity after invoking Taylor's hypothesis. The amplification ratio $G_\lambda = \frac{\lambda_{x,d}}{\lambda_{x,u}}$ is plotted in figure 49 together with the amplification of the same scale λ_ϵ obtained from:

$$\epsilon = \frac{\overline{u^2}}{\lambda_\epsilon^2}$$

The data clearly indicate that Taylor's microscale increases after the interaction.

Amplification of pressure fluctuations is not the same for all distances away from the grid. Figure 50 shows the effect of amplification of pressure fluctuations for three different grids. The 10x10 grid generated higher pressure fluctuations than the other two grids (4x4, 2x2) and thus amplification was higher. From the same picture one can also depict the amplification of pressure fluctuations at relatively large downstream distances. It is interesting to point out that at large non-dimensional distances (non-dimensionalized with the grid size) x/M=720 the pressure fluctuations are still amplified.

10. CONCLUDING REMARKS

The interaction of an isotropic and homogeneous turbulent flow with a strong axisymmetric disturbance, like a normal shock, is the best paradigm of a test case where a turbulence model of the LES or RANS class can be evaluated. The absence of turbulence production and the simplified flow geometry can expose the model's strengths and weaknesses.

Experimental realization of a homogeneous and isotropic flow interacting with a normal shock in the laboratory is a formidable task. There are two major difficulties associated with this: Setting up a compressible and isotropic turbulent flow is the first one and the generation of a normal shock interacting with flow is the second. These two problems may be interrelated and may be not independent from each other. As a result of these difficulties two different categories of experiments have been carried out. The experimental set up in shock tubes offers the possibility of unsteady shock interactions with isotropic turbulence of various length scales and intensity.

a. Compressibility effects in the incoming flow

The effects of compressibility in a nearly homogeneous and nearly isotropic flow of decaying turbulence have been investigated experimentally by carrying out high resolution measurements in a large scale shock tube research facility. A variety of grids of rectangular mesh size was used to generate the flow field. The Reynolds number of the flow based on the mesh size Re_M was ranging from $50x10^3$ to $400x10^3$ while the turbulent Reynolds number Re_λ based on Taylor's microscale λ was between 200 and 700 which constitutes one of the highest ever achieved in laboratory scale flow. The range of Mach number of the flows investigated was between 0.3 and 0.6 which was low enough to assure a shock free flow and reasonably high enough to contain compressibility effects.

The isotropy of the present flow was verified experimentally and it was found to be within the range reported for incompressible flows. In fact, it was established for the first time that isotropic compressible turbulence at moderate subsonic Mach numbers can be setup experimentally. The decay of Mach number fluctuations was found to follow a power law similar to that describing the decay of incompressible isotropic turbulence

$$M_t^2 = B\left[\frac{x}{M} - \left(\frac{x}{M}\right)_0\right]^{-n}$$

where B, $(x/M)_0$ and n are constants depending on the flow Mach number as well as on the Re_M. It was possible to investigate the effects of the Mach number and Re_M on the flow development independently from each other. The decay coefficient B and the decay exponent n decrease with increasing Mach number while the virtual origin $(x/M)_0$ increases with increasing Mach number.

Most probably the mechanism responsible for this effect is the inherently low growth rate of compressible shear layers emanating from the cylindrical rods of the grid. Figure 51a shows a typical merging of shear layers to form an isotropic flow in the case of incompressible flows. The case of compressible shear layers is depicted in figure 51b where it is shown how a lower growth rate can result in longer virtual origin. If a shock wave had been formed in the vicinity of the grid as in the case of Zwart et al. (1996) the decay rate would have been drastically affected. Shock waves in the present case is more likely to appear at Mach numbers higher than 0.7 because the open area of the grids used is greater than that required to choke the flow through the grids. Therefore it is plausible to attribute the present results to the lower growth rate of compressible shear layers.

The Taylor's microscale appears also to increase with increasing Mach number. The Kolmogorov's length scale η decreases as the Mach number of the flow increases. The results also indicated that η increases as the mesh size increases

Table 2, presented at the end of this section, summarizes the conclusions for the parameters that were investigated in this work and their response to an increase of the mean flow Mach number and an increase in the mesh size/Re_M. In this table three symbols are used: (↑) represents that the parameter increases with increasing M_{flow} or increasing mesh size/Re_M. (↓) represents that the parameter decreases with increasing M_{flow} or increasing mesh size/Re_M and finally (↕) represents that the parameter because of compressibility effects does not present a specific trend with increasing M_{flow} or increasing mesh size/Re_M.

b. The interaction with the shock

An experimental study of the interaction of a normal shock wave with decaying grid generated nearly isotropic turbulence has been performed using time resolved pressure, velocity, temperature and Mach number measurements in a shock tube. Spatial resolution of the order of 7-26 Kolmogorov viscous length scales was achieved in the measurements of turbulence. A variety of turbulence generating grids provide a wide range of turbulence scales with flow Mach numbers ranging from 0.3 to 0.7 and shock Mach numbers from 1.2 to 1.6.

The present results verified a proposed power law decay of the turbulent Mach number M_t in the range of 0.01 to 0.1. Longitudinal velocity fluctuations were amplified through the shock.

The results show that the decay exponent, n, is a function of the mesh size i.e. initial conditions before the interaction, and that its value is substantially less than one. The effect of the shock interaction is very dramatic and produces a dependance of n on the M_s, M_{flow} and initial conditions. The decay exponent after interaction is greater than the one obtained before interaction for all investigated cases.

Amplification of velocity fluctuations after the interaction was found in all case involving turbulence produced by coarse grids. This amplification increases with shock strength and flow Mach number. In the case of fine grids, amplification was found in all interaction with low M_{flow} while at higher M_{flow} reduced or no amplification of turbulence was evident. These results indicate that the outcome of the interaction depends strongly on the upstream properties of the flow.

Integral length scales in the longitudinal direction were reduced after the interaction in all investigated flow cases. The same length scales in the normal direction increased at low Mach numbers and decrease during stronger interactions. It appears that at the weakest of the present interactions the eddies are compressed in the longitudinal direction drastically while their extent in the normal direction remains relatively the same. As the shock strength increases the lateral length scale increases while the longitudinal decreases. At the strongest interaction of the present cases the eddies are compressed in both directions. However, even at the highest Mach number case the issue is more complicated since amplification of the lateral scales has been observed in fine grids. Thus the outcome of the interaction strongly depends on the initial conditions. The dissipation rate was reduced through the interaction while all dissipative length scales were found to increase. DNS results of Lee et al. (1994) have indicated a small increase of dissipative length scales through weak shock interactions. For shock strengths greater than 1.25 DNS predicts a substantial decrease in L_ϵ. The Re_λ of the DNS was between 12 and 22 which is considered lower than that in the present experiments and may be the cause of this disagreement between experiments and DNS.

The present results clearly show most of the changes, either attenuation or amplification occur at large x/M distances where the length scales of the incoming flows are high and turbulence intensities low. Thus large in size eddies with low velocity fluctuations are affected the most by the interaction with the shock.

Table 3 summarizes in a similar fashion as before the conclusions for the parameters that were investigated in this work and their response to an increase of the mean flow Mach number and an increase in the mesh size/Re_M.

REFERENCES

Adamson, T.C. and Messiter, A.F., 1980, "Analysis of two Dimensional Interactions Between Shock Waves and Boundary Layers", Ann. Rev. Fluid Mech., vol.12, 103.

Agui, J., 1998, "Vorticity transfer through shock waves," PhD Thesis, City University of New York, (in preparation).

Alem, D., 1995, "Analyse experimentale d'une turbulence homogene en ecoulement supersonoc soumise a un choc droit", These de doctorat, Univerite de Poitiers.

Andreopoulos, J. and Muck, K.C., 1987, "Some New Aspects of the Shock-Wave Boundary Layer Interaction in Compression Ramp Corner", J. Fluid Mech., vol.180, 405.

Ardonceau, P.L., 1984, "The Structure of Turbulence in a Supersonic Shock-Wave/Boundary Layer Interaction", AIAA J., vol.22 (9), 1254.

Anyiwo, J.C. and Bushnell, D.M., 1982, "Turbulence Amplification in Shock-Wave Boundary Layer Interaction", AIAA J., vol.20, 893.

Barre, S., Allem, D., and Bonnet, J. P., 1996, "Experimental study of normal shock/homogeneous turbulence interaction", AIAA J., vol. 34(5), pp. 968-974.

Blin, E., 1993, "Etude experimentale de l'interaction entre turbulence libre et une onde de choc", These de doctorat, Universite Paris 6.

Briassulis, G.K., 1996, "Unsteady Nonlinear Interactions of Turbulence with Shock Waves", Ph.D. Thesis, City College of CUNY.

Batchelor, G. K., and Townsend, A. A., 1949, " The Nature of Turbulent Motion at High Wave Numbers," Proc. Roy. Soc. A, 199, 238.

Bennett J. C. and Corrsin S., 1978, "Small Reynolds Number Nearly Isotropic Turbulence in a Straight Duct and Contraction," Phys. Fluids, 21 (12), 2129.

Betchov, R. and Lorenzen, C., 1974, "Phase Relations in Isotropic Turbulence," Phys. Fluids, 17 (8), 1503.

Briassulis, G., Honkan, A., Andreopoulos, J., and Watkins, B. C., 1995, "Applications of Hot-Wire Anemometry in Shock Tube Flows," Exp. in Fluids, vol 19, 29.

Buckingham, A., C., 1990, "Interactive Shock Structure Response to Turbulence," AIAA Paper No 90-1642.

Budwig, R., Zwart, P., J., Nguyen, V., and Tavoularis, S., "Grid Generated Turbulence in Compressible Streams," ASME, 2nd Symp. on Transitional and Turbulent Compressible Flows, Aug. 1995.

Cambon, C., Coleman, G.N., and Mansour, N.N., 1993, "Rapid distortionanalysis and direct simulation of compressible homogeneous turbulence at finite Mach number", J. Fluid Mech., vol. 257, pp. 641-665.

Chu, B.T. and Kovasznay, L.S.G., 1957,"Non-linear Interactions in a viscous Heat-Conducting Compressible Flow", J. Fluid Mech., vol.3, 494.

Debieve, J.F. and Lacharme, J.P., 1985, "A Shock Wave Free Turbulence Interactions", IUTAM Conference, Paris.

Dosanjh, D.S. and Weeks, T.M., 1964, "Interaction of a Starting Vortex as well as Karman Vortex Streets with Traveling

Shock Wave", AIAA Paper No. 64-425.

Favre, A., 1965, "Equations des Gaz Turbulents Compressibles I," J. Méc., vol 4, 361.

Frenkiel, F., N., and Klebanoff, P., H., 1971, "Statistical Properties of Velocity Derivatives in Turbulent Field," J. Fluid Mech., vol. 48, 183.

Frenkiel, F., N., Klebanoff, P., H., and Huang, T., T., 1979, "Grid Turbulence in Air and Water," Phys. Fluids, 22 (9), 1606.

Gutmark, E., J., Schadow, K., C., and Yu, K., H., 1995, "Mixing Enhancement in Supersonic Free Shear Flows," Annu. Rev. Fluid Mech., vol. 27, 375.

Haas, J.F., and Sturtevant, B., 1987, "Interaction of Weak Shock Waves with Cylindrical and Spherical Gas Inhomogeneities", J. Fluid Mech., vol.181, 41.

Hannappel, R., and Fridrich, R., 1995, "Interaction of isotropic turbulence with a normal shock-wave", Appl. Sci. Res., Vol. 54, pp. 205-221.

Hancock, P. E. and Bradshaw P., 1983, "The Effect of Free-Stream Turbulence on Turbulent Boundary Layers," J. Fluid Eng., vol. 105, 284.

Hayakawa, K., Smits, A. J., and Bogdonoff, S. M., 1984, "Turbulence Measurements in a Compressible Reattaching Shear Layer," AIAA Journal, vol. 22, 889.

Hartung, L.C. and Duffy, R.E., 1986, "Effects of Pressure on Turbulence in Shock-Induced Flows", AIAA Paper No 86-0127.

Hesselink, L. and Sturtevant, B., 1988, "Propagation of Weak Shocks Through Random Medium", J. Fluid Mech., vol.196, 513.

Honkan, A. and Andreopoulos, J., 1992, "Rapid Compression of Grid-Generated Turbulence by a Moving Shock Wave", Phys. Fluids A, 4 (11).

Honkan, A. and Andreopoulos, J., 1997, "Vorticity strain-rate and dissipation characteristics in the near wall region of turbulent boundary layers", J. Fluid Mech., vol. 350, pp. 29-96.

Honkan, A., Watkins, C.B., and Andreopoulos, J., 1993, "Experiments of Shock Wave Interactions with Free Stream Turbulence", ASME Fluids Engineering Conference, Washington D.C.

Honkan, A. Watkins C. B. and Andreopoulos, J., 1994, "Experimental Study of Interactions of Shock Wave with Free Stream Turbulence" , J. Fluids Eng., vol. 116, 763.

Hunt, J.R.C., 1973, "A Theory of Turbulent Flow Round Two-Dimensional Bluff Bodies", J. Fluid Mech., vol.61, 625.

Jacquin, Blin and Geffroy , 1993, "En Experimental Study on Free Turbulence/Shock Wave Interaction" , VIII Turbulent Shear Flows (eds: Durst et al), pp 229-248, Springer Verlag.

Keller, J. and Merzkirch, W., 1990, "Interaction of a Normal Shock with a Compressible Turbulent Flow", Exp. Fluids 8, 241.

Kistler, A., L., and Vrebalovich, T., 1966, "Grid Turbulence at large Reynolds numbers," J. Fluid Mech., vol. 26, 37.

Kuo, A. Y., and Corrsin, S., 1971, "Experiments on Internal Intermittency and Fine Structure Distribution Functions in Fully

Turbulent Flows," J. Fluid Mech., vol. 50, 285.

Lee, L. and Lele, S.K. and Moin, P., 1991, "Direct Numerical Simulation and Analysis of Shock Turbulence Interaction", AIAA Paper No 91-0523.

Lee, L., Lele, S. K. and Moin, P., 1993, "Direct Numerical Simulation of Isotropic Turbulence Interacting with a Weak Shock Wave", J. Fluid Mech., vol. 251, 533.

Lee, L., Lele, S. K. and Moin, P., 1994, "Interaction of Isotropic Turbulence with a Strong Shock Wave," AIAA Paper No 94-0311.

Mahesh, K., Lele, S.K.,and Moin, P., 1997, "The influence of entropy fluctuationson the interaction of turbulence with a shock wave", J. Fluid Mech., vol. 334, pp353-379.

Mc Kenzie, J. F. and Westphal, K. O., 1968, "Interaction of Linear Waves with Oblique Shock Waves", Phys. of Fluids, vol. 11, No 11, 2350

Mills, R. R., Kistler, A., L., O'Brien, V., and Corrsin, S., 1958, "Turbulence and Temperature Fluctuations Behind a Heated Grid," N.A.C.A. Tech. Note No. 4288.

Mohamed, S. M., and LaRue, C. J., 1990, "The Decay Power Law in Grid Generated Turbulence," J. Fluid Mech., vol. 219, 195.

Morkovin M.V., 1960, "Note on Assessment of Flow Disturbances at a Blunt Body Traveling at Supersonic Speeds Owing to Flow Disturbances in Free Stream" J. Applied Mechanics, vol. 27, 223.

Ribner, H.S., 1955, "Convection of a Pattern of Vorticity Through a Shock Wave," NACA Rept. 1233.

Ribner, H. S., 1986, "Spectra of Noise and Amplified Turbulence Emanating from Shock-Turbulence Interaction," AIAA Journal, vol. 25, 436.

Rotman, D., 1991, "Shock Wave Effects on a Turbulent Flow," Phys. Fluids A, 3 (7).

Samimy M., and Addy A.L., 1985, "A Study of Compressible Turbulent Reattaching Free Shear Layers" AIAA Paper 85-1646.

Samimy, M., Petrie, H. L., and Addy, A. L., 1986, "A Study of Compressible Turbulent Reattaching Free Shear Layers," AIAA Journal, vol. 24, 261.

Sekundov, A.N., 1974, "Supersonic Flow Turbulence and Interaction With a Shock Wave," Izv. Akad. Nauk SSR Mekh. Zhidk. Gaza, March - April.

Settles, G.S., Fitzpatrick, T.J. and Bogdonoff, S.M., 1979, "Detailed Study of Attached and Separated Compression Corner Flow Fields in High Reynolds Numbers Supersonic Flow," AIAA J., vol. 17(5), 579.

Settles, G.S., Williams, D.R., Baca, B.K. and Bogdonoff, S.M., 1982, "Reattachment of a Compressible Turbulent Free Shear Layer," AIAA J., vol. 20, 60.

Smits S.J., and Muck K.C., 1987,"Experimental study of three shock wave/boundary layer interactions," J. Fluid Mech.,vol.182, pp 291-314.

Spina, E., F., Smits, A., J., and Robinson, S., K., 1994, "The Physics of Supersonic Turbulent Boundary Layers," Annu. Rev. Fluid Mech., vol. 26, 287.

Stewart, R. W., and Townsend, A. A., 1951, "Similarity and Self Preservation in Isotropic Turbulence," Proc. Roy. Soc. A, 243, 359.

Tan-Atichat, J., Nagib, H., M., and Loehrke, R., I., 1982, "Interaction of Free-Stream Turbulence with Screens and Grids: A Balance between Turbulence Scales," J. Fluid Mech., vol. 114, 501.

Tavoularis S., Bennett J. C. and Corrsin S., 1978, "Velocity derivative skewness in small Reynolds number, nearly isotropic turbulence," J. Fluid Mech., vol. 88, 63.

Tennekes, H. and Lumley, J. L., 1972. "A First Course in Turbulence", Boston, MA., MIT press .

Trolier J.W. and Duffy, R.E., 1985, "Turbulent Measurements in Shock-Induced Flows," AIAA J., vol. 23(8), 1172.

Tsinober, A., Kit, E., and Dracos, T., 1992, "Experimental Investigation of the Field of Velocity Gradients in Turbulent Flows," J. Fluid Mech., vol. 242, 169.

Zang T.A., Hussaini, and Bushnell, D.M., 1982, "Numerical Computations of Turbulence Amplification in Shock Wave Interactions," AIAA Paper 82-0293.

Zwart, P., Budwig, R., and Tavoularis, S., 1996, "Grid Turbulence in Compressible Flow," private communication.

Grid (Meshes/in)	Mesh size M (mm x mm)	Incident Shock M_s	Reflected Shock M_r	Flow Mach # M_{flow}	Re_M	Re_λ
8x8	3.18x3.18	1.27	1.18	0.371	37138	162
8x8	3.18x3.18	1.342	1.25	0.461	53506	195
8x8	3.18x3.18	1.486	1.392	0.592	63458	246
5x5	5.1x5.1	1.27	1.18	0.371	59654	222
5x5	5.1x5.1	1.367	1.26	0.477	86315	250
5x5	5.1x5.1	1.469	1.388	0.576	102421	325
4x4	6.35x6.35	1.254	1.175	0.354	68208	223
4x4	6.35x6.35	1.337	1.242	0.446	105389	277
4x4	6.35x6.35	1.489	1.393	0.594	132921	355
3x3	8.5x8.5	1.227	1.166	0.321	81687	224
3x3	8.5x8.5	1.364	1.258	0.474	124203	316
3x3	8.5x8.5	1.456	1.372	0.564	215043	654
2x2	12.7x12.7	1.248	1.17	0.346	137319	267
2x2	12.7x12.7	1.328	1.231	0.436	169025	405
2x2	12.7x12.7	1.486	1.392	0.592	261667	737
1.33x1.33	19.05x19.05	1.267	1.179	0.368	200371	270
1.33x1.33	19.05x19.05	1.394	1.278	0.504	295721	550
1.33x1.33	19.05x19.05	1.504	1.405	0.607	398661	680
1x1	25.4x25.4	1.274	1.184	0.376	256903	296
1x1	25.4x25.4	1.42	1.291	0.529	438727	582
1x1	25.4x25.4	1.622	1.475	0.708	577040	735

Table 1: Bulk flow parameters of the experiments performed.

	INCREASING M_{flow}	INCREASING Re_M/M
A	⇓	⇕
$(x/M)_0$	⇑	⇓
n	⇓	⇕
u	⇑	⇕
M_t	⇑	⇕
ϵ	⇑	⇕
$\epsilon M/U^3$	⇑	⇕
L_e	⇑	⇑
λ	⇑	⇑
η	⇓	⇑
$L_{11}(\xi_1)$	⇕	⇓
$L_{11}(\xi_2)$	⇓	⇕

Table 2: Summary of conclusions for the decaying isotropic flowfield.

	INCREASING M_{flow}	INCREASING Re_M/M	SHOCK WAVE INTERACTION
A	⇕	⇕	⇑
$(x/M)_0$	⇑	⇓	⇑
n	⇕	⇕	⇑
u	⇓	⇓	⇕
M_t	⇑	⇕	⇕
ϵ	⇕	⇓	⇓
$\epsilon M/U^3$	⇓	⇓	⇑
L_e	⇑	⇑	⇑
λ	⇕	⇑	⇑
η	⇕	⇑	⇑
$L_{11}(\xi_1)$	⇕	⇑	⇓
$L_{11}(\xi_2)$	⇓	⇓	⇕

Table 3: Summary of conclusions for the interaction of a decaying isotropic flowfield with a planar shock wave.

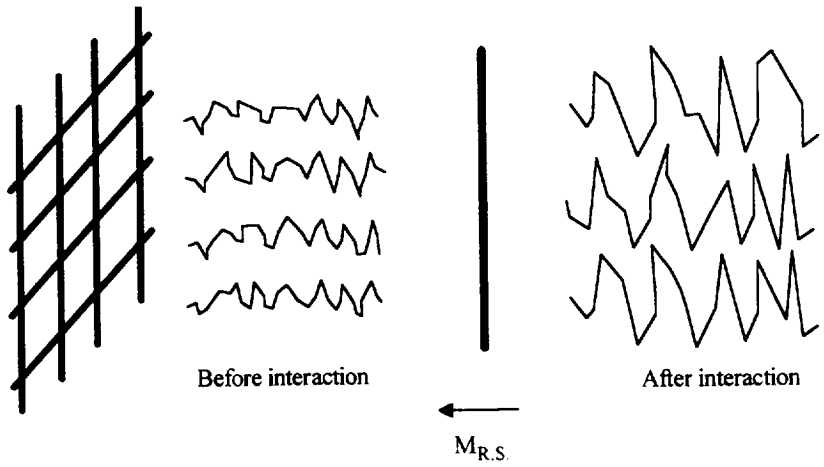

Figure 1a: Shock wave interaction with grid turbulence.

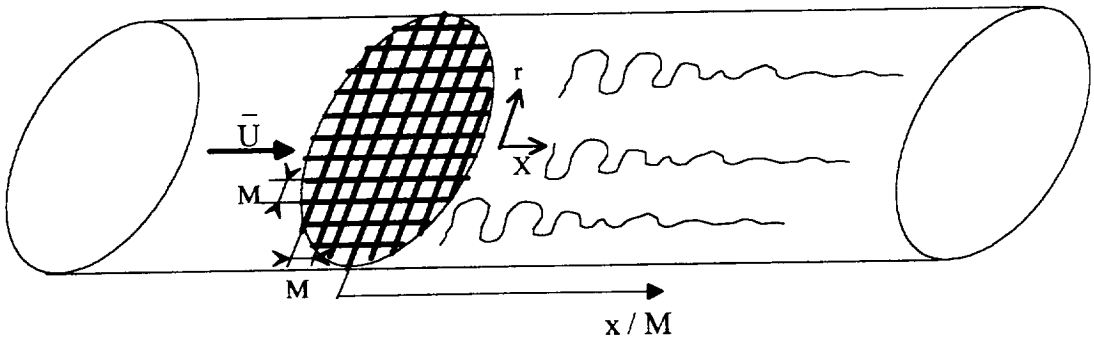

Figure 1b: Grid generated flow schematic.

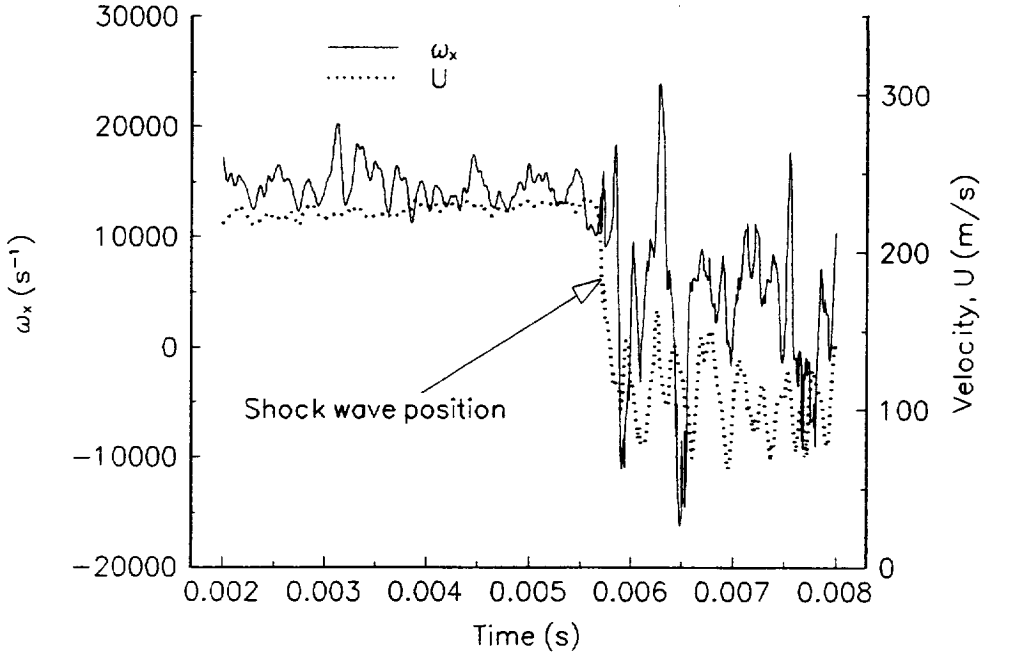

Figure 1c: Velocity and vorticity signals through the interaction with shock

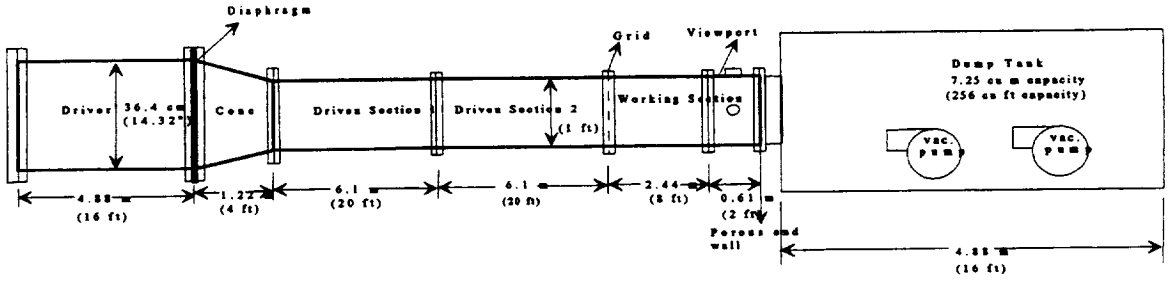

Figure 2: The new shock tube facility (not to scale)

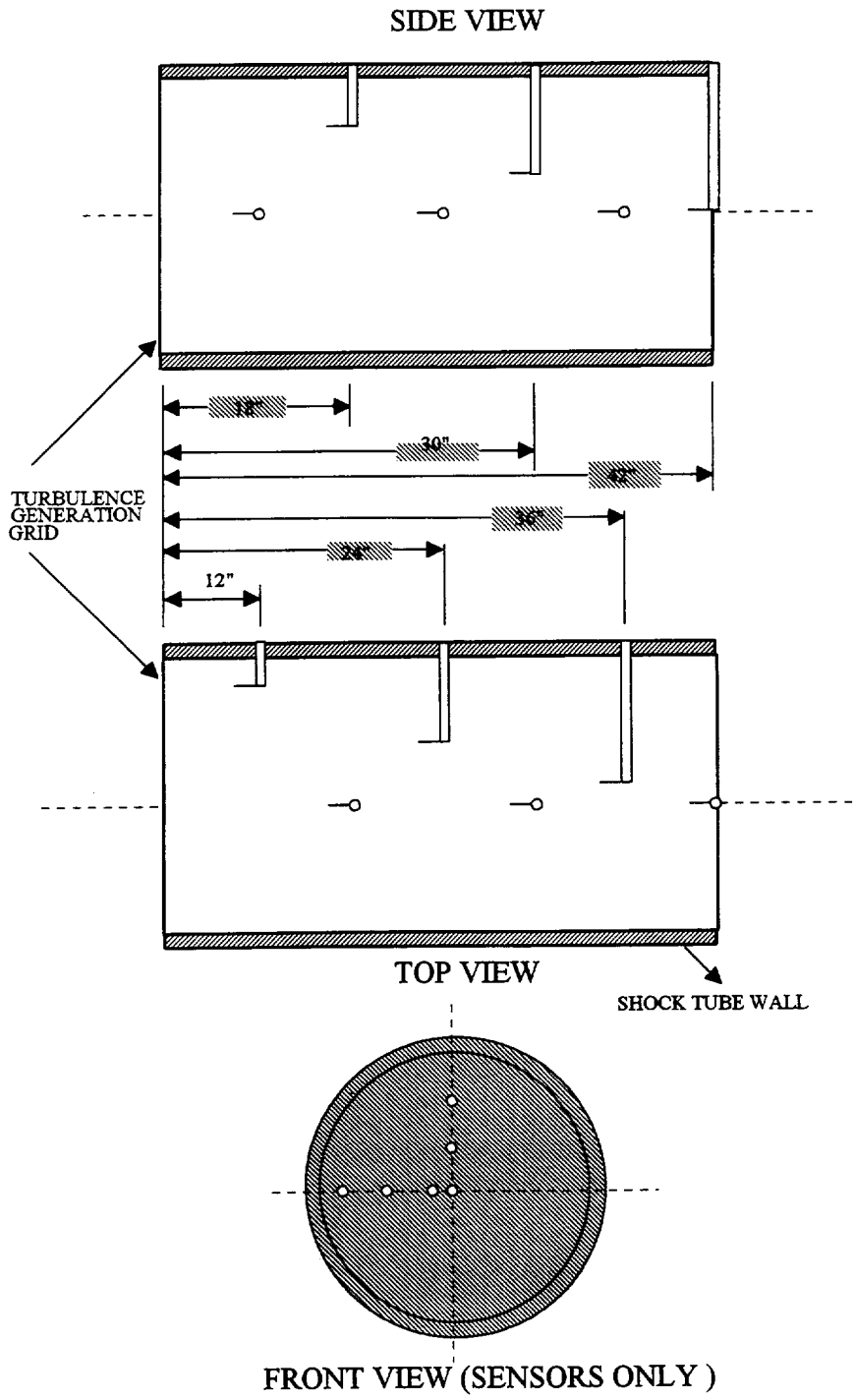

Figure 3: X-Wire probe location and arrangement in the shock tube.

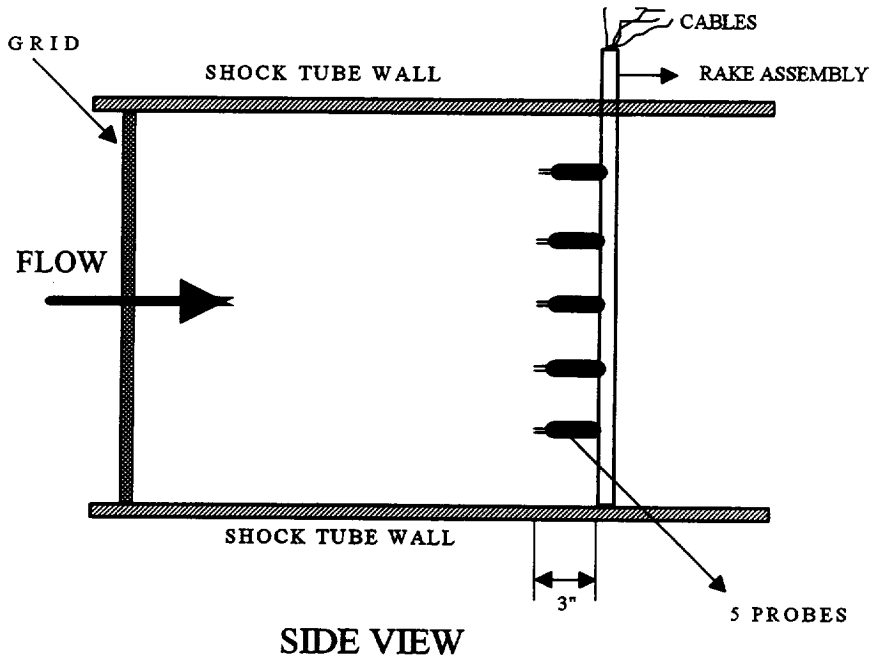

Figure 4: Side view of the rake assembly in the shock tube.(not to scale)

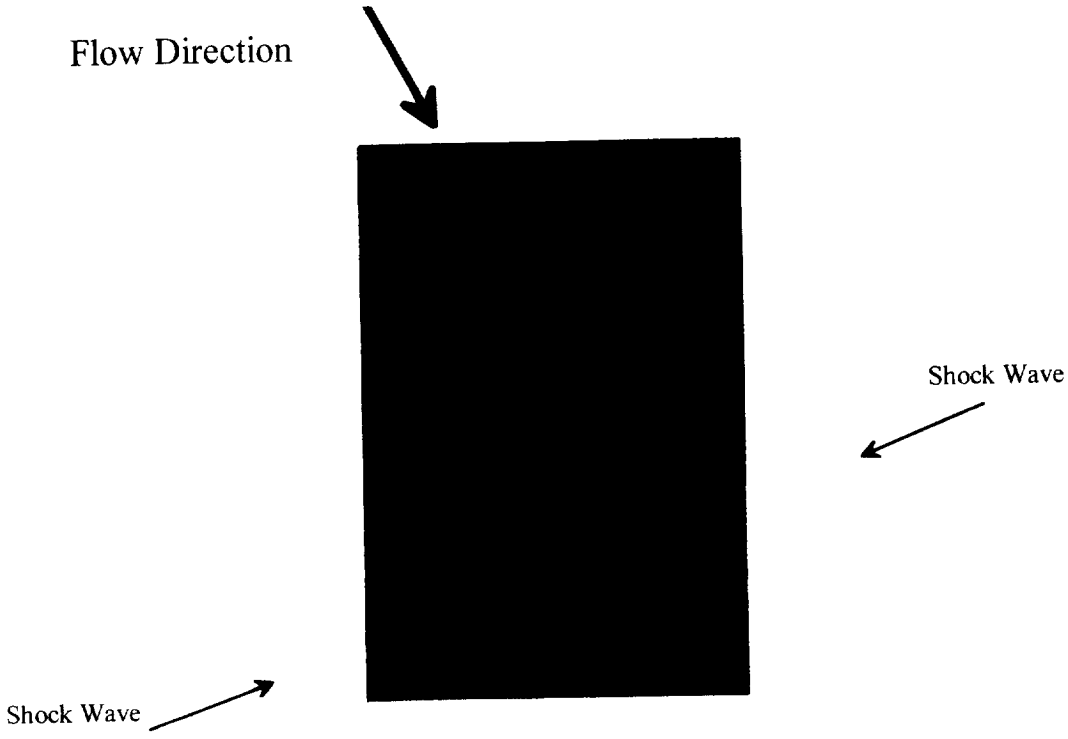

Figure 5: Shock wave visualization

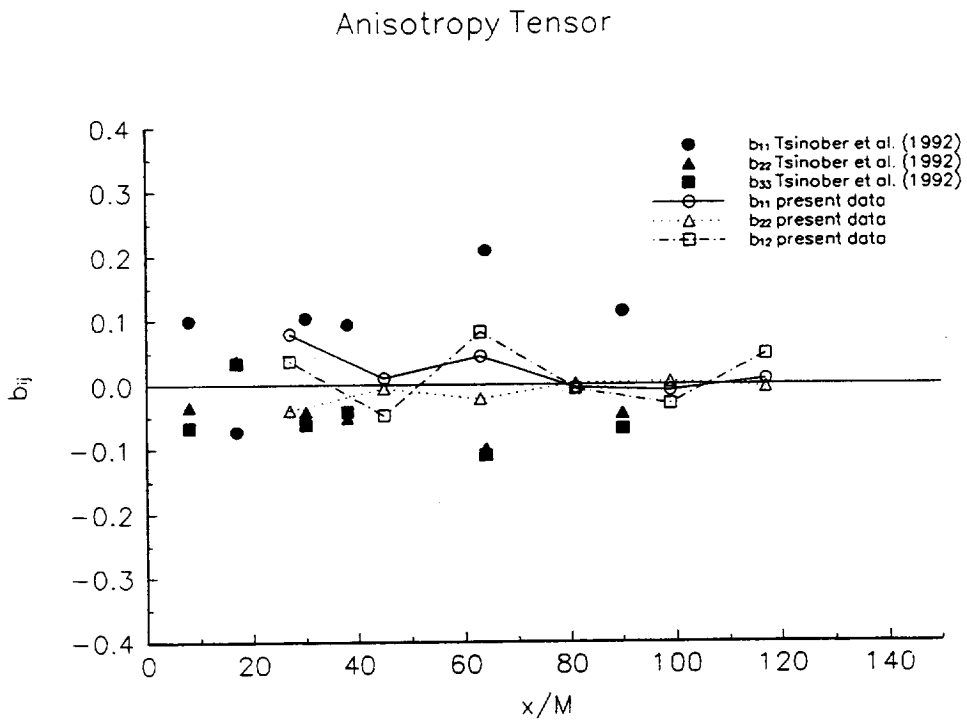

Figure 6: Anisotropy Tensor b_{ij} vs x/M

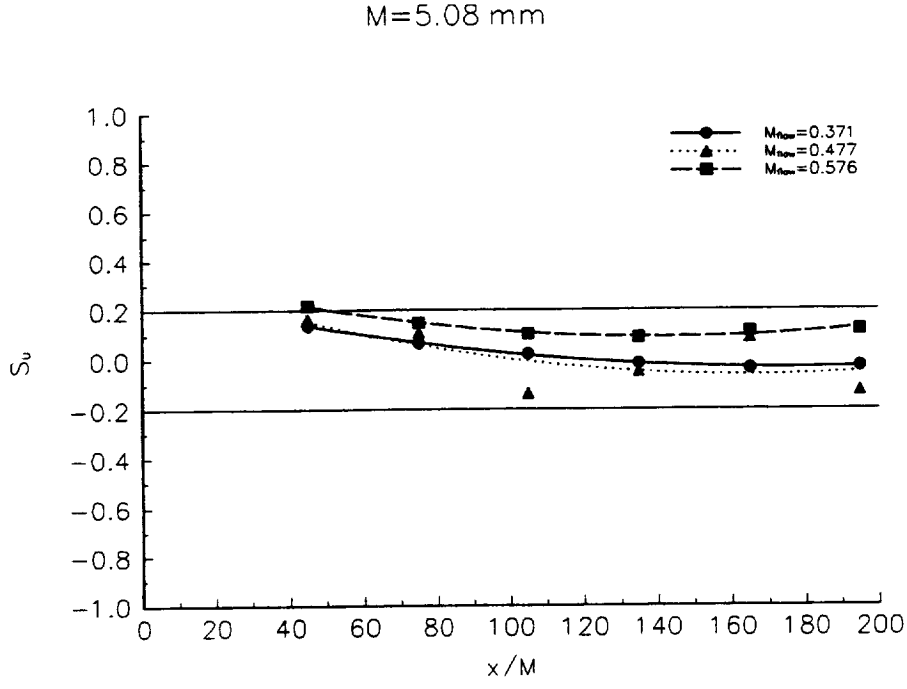

Figure 7: Skewness of velocity fluctuations for three different flowfields.

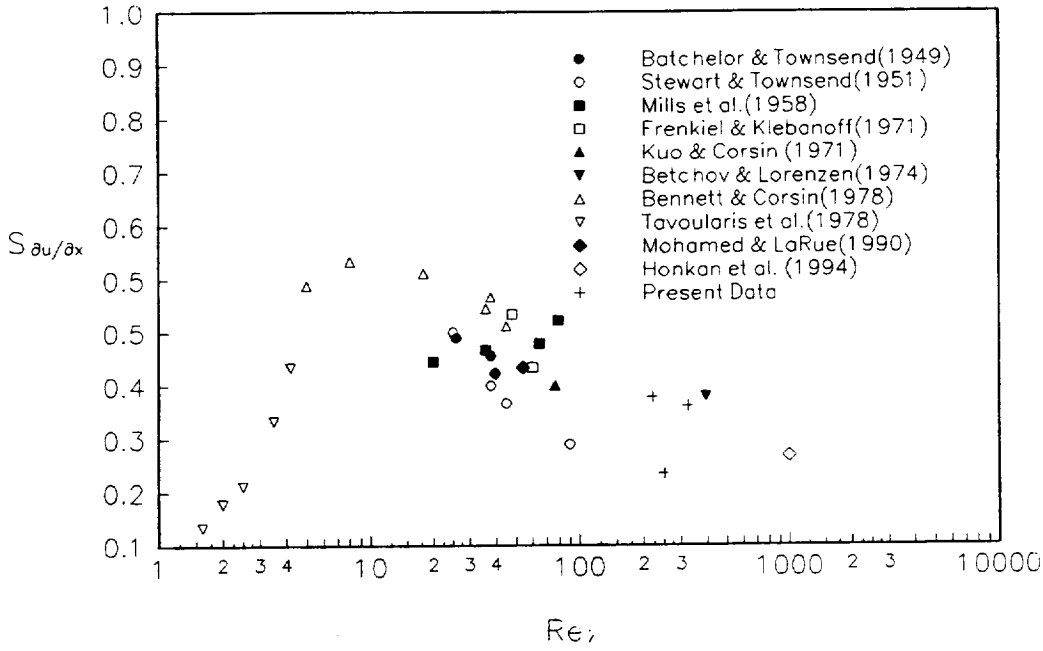

Figure 8: Skewness of the derivative of velocity fluctuations for different flowfields.

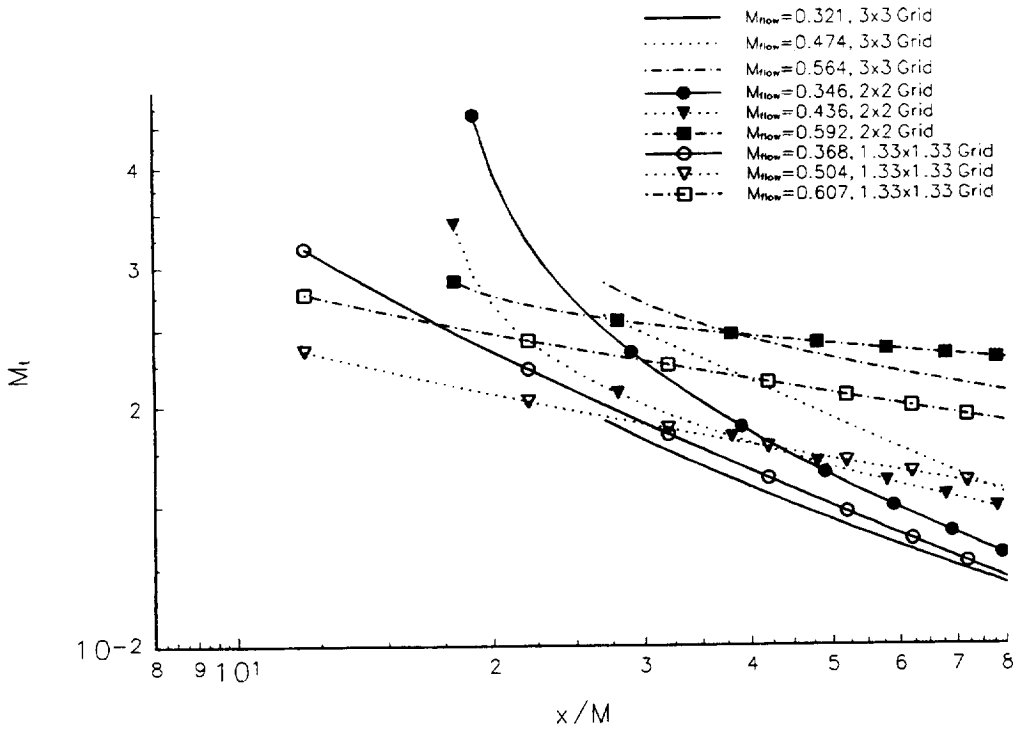

Figure 9: Mach number fluctuations for various experiments

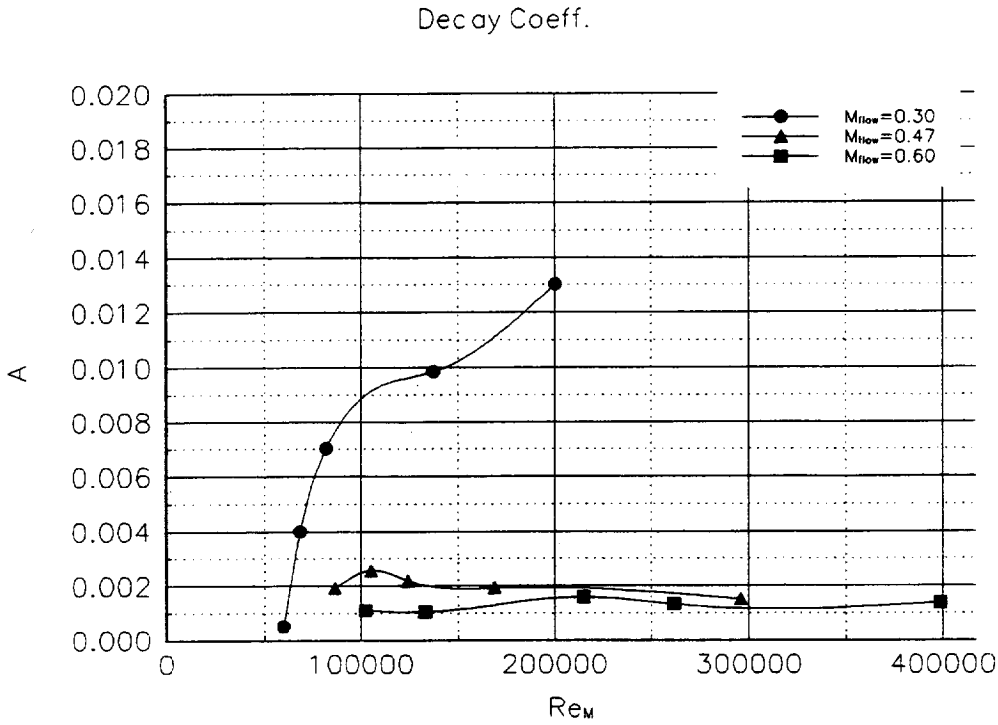

Figure 10: Decay coefficient A vs Re_M for 3 different Mach numbers

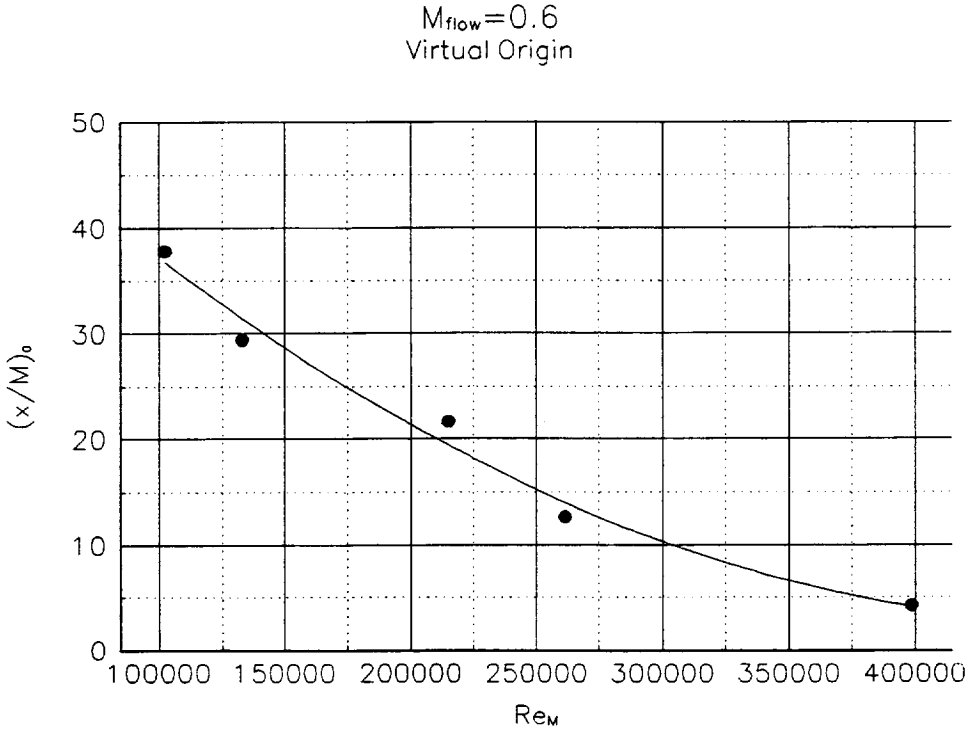

Figure 11: Virtual origin vs Re_M for M_{flow}=0.6

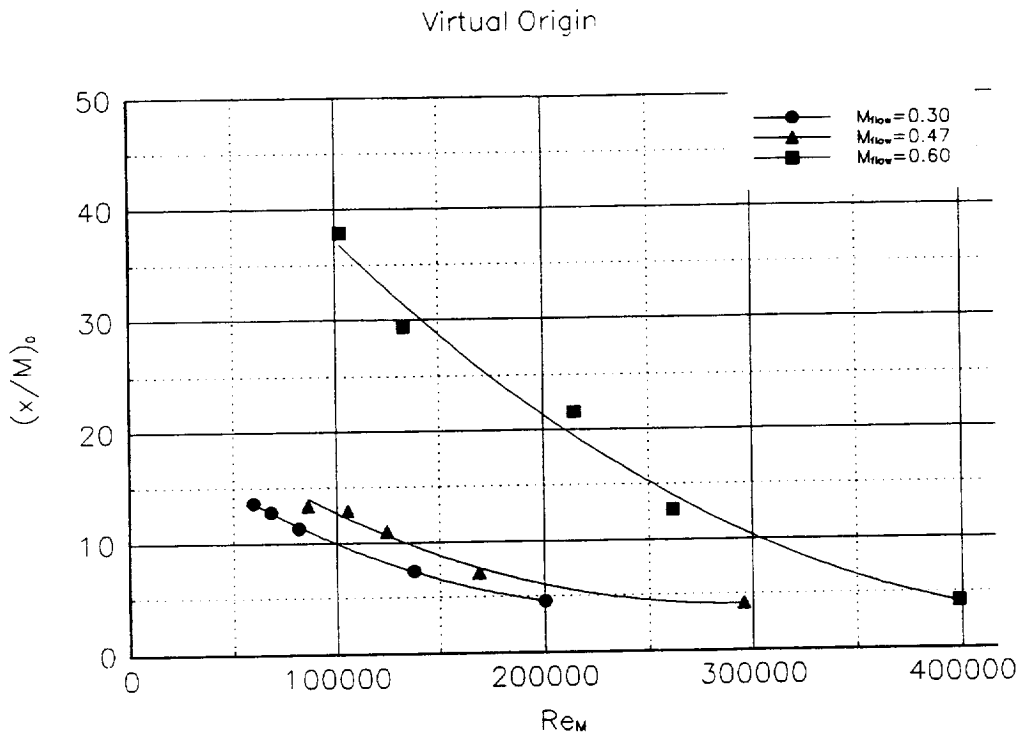

Figure 12: Virtual origin vs Re_M for 3 different Mach numbers

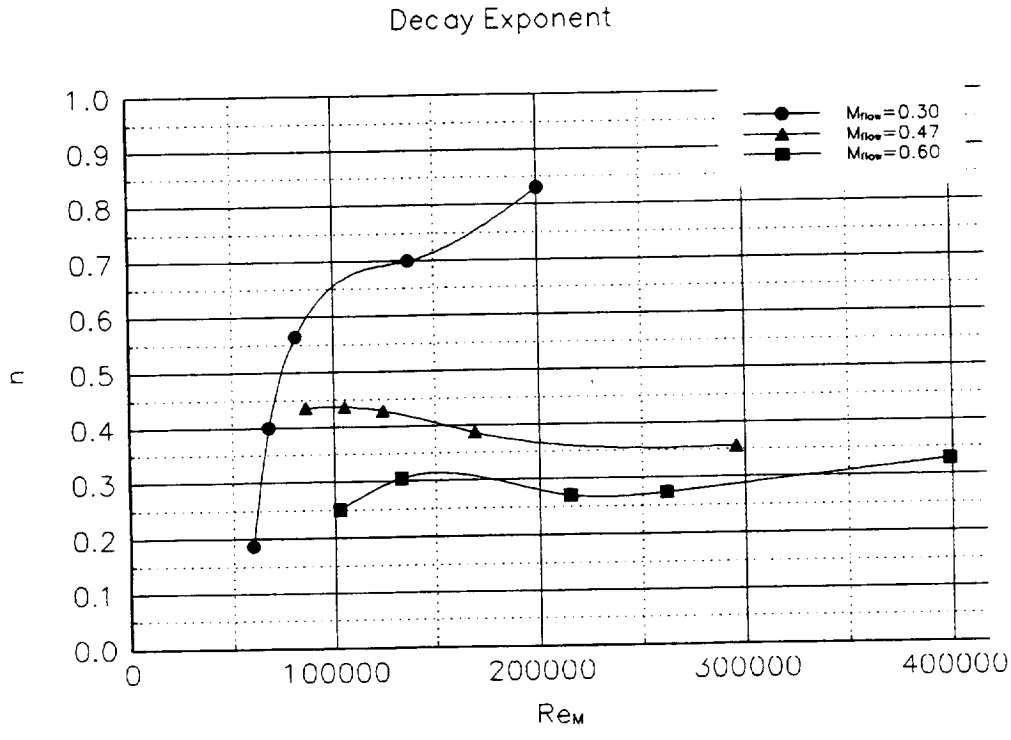

Figure 13: Decay exponent n vs Re_M for 3 different Mach numbers

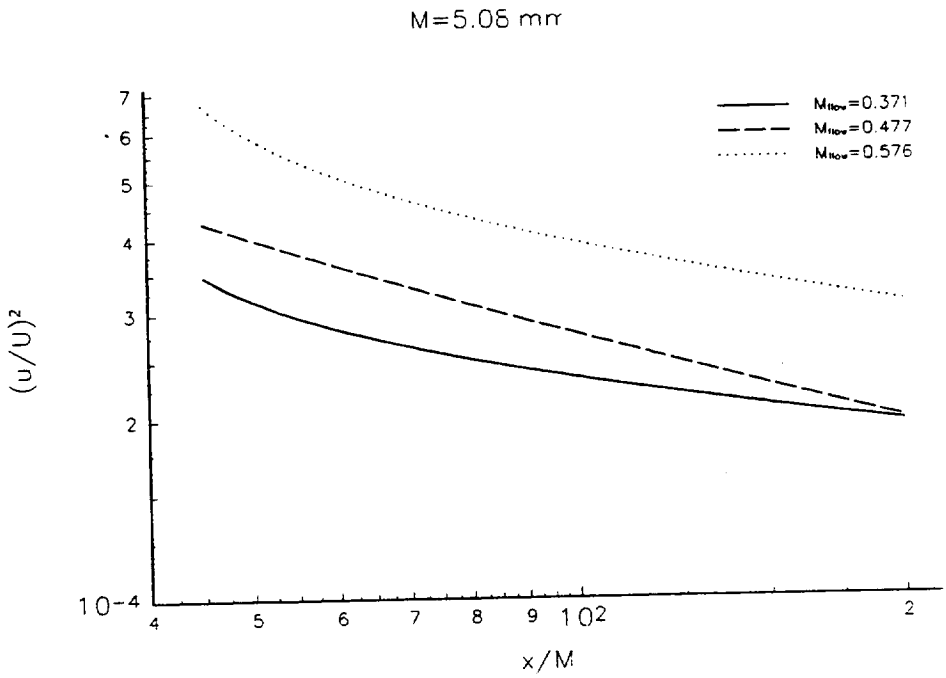

Figure 14: Decay of velocity fluctuations for various Mach numbers

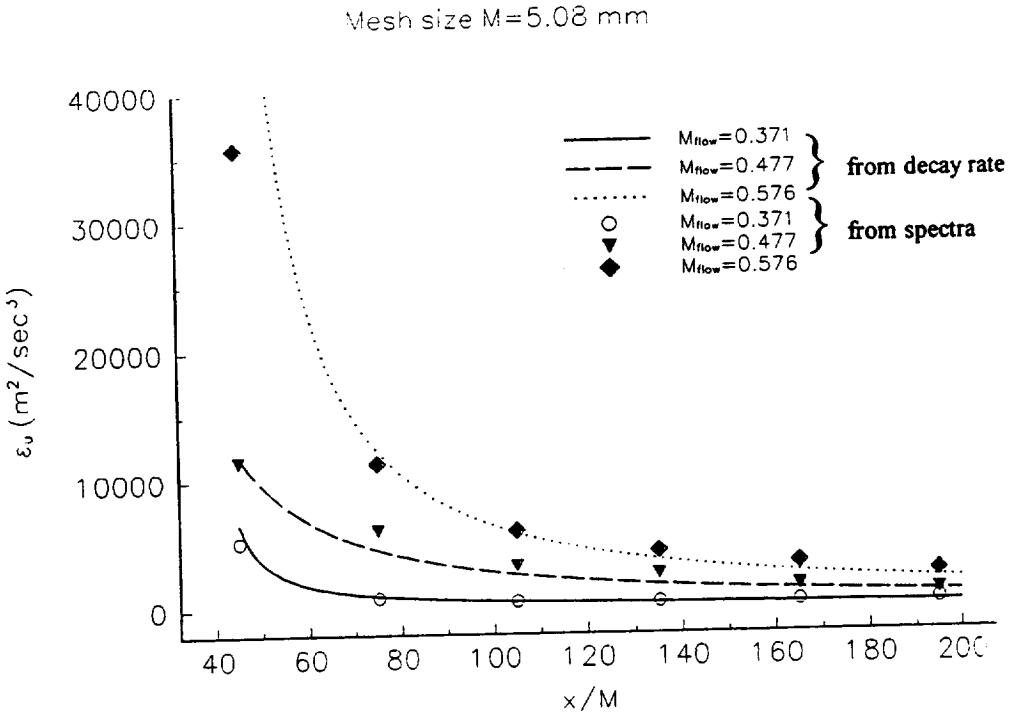

Figure 15: Dissipation rate of kinetic energy vs x/M for 3 different Mach numbers

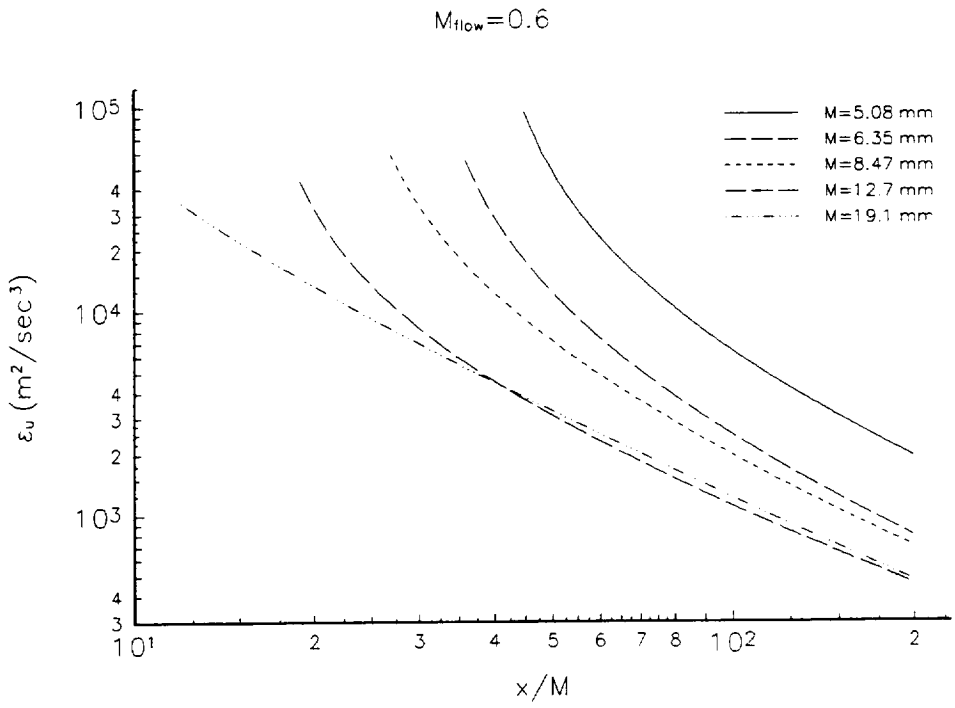

Figure 16: Dissipation rate of kinetic energy for various mesh sizes.

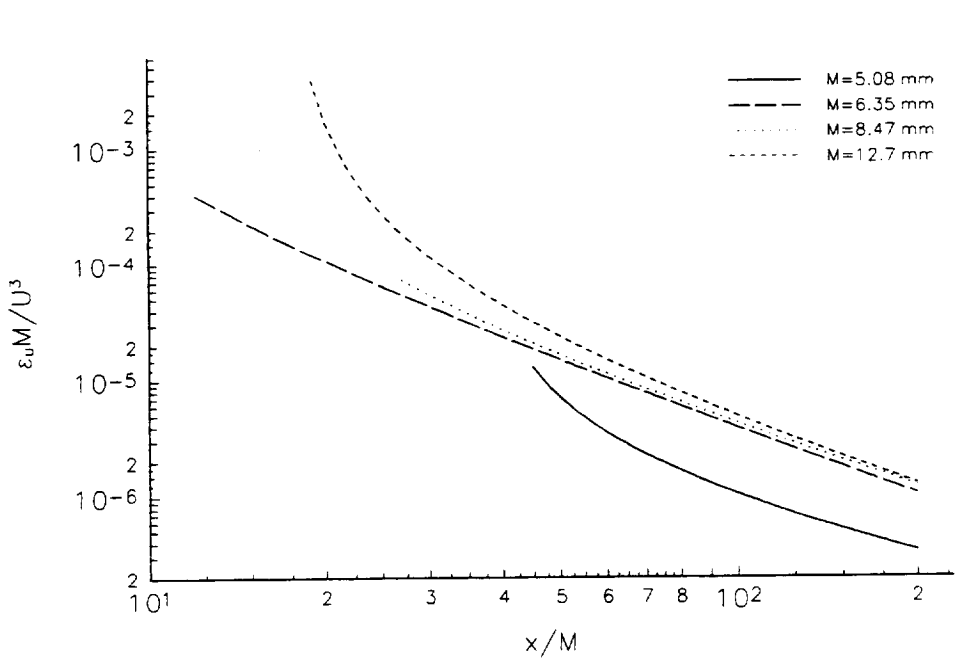

Figure 17: Non dimensional ϵ for M_{flow}=0.35 and various mesh sizes.

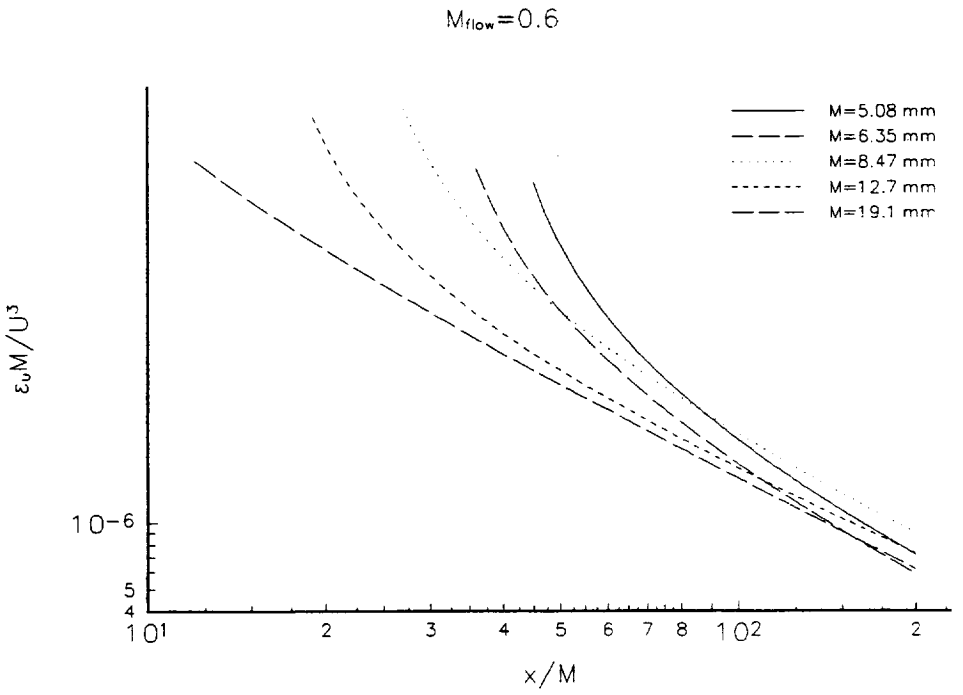

Figure 18: Non dimensional ϵ for M_{flow}=0.6 and various mesh sizes.

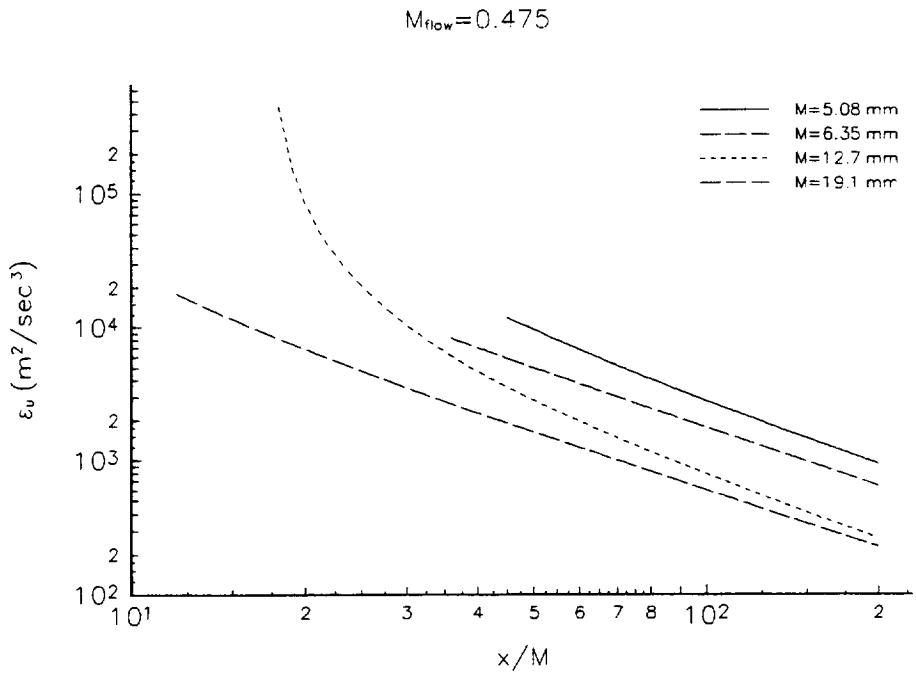

Figure 19: Dissipation rate of kinetic energy for various mesh sizes at M_{flow}=0.475

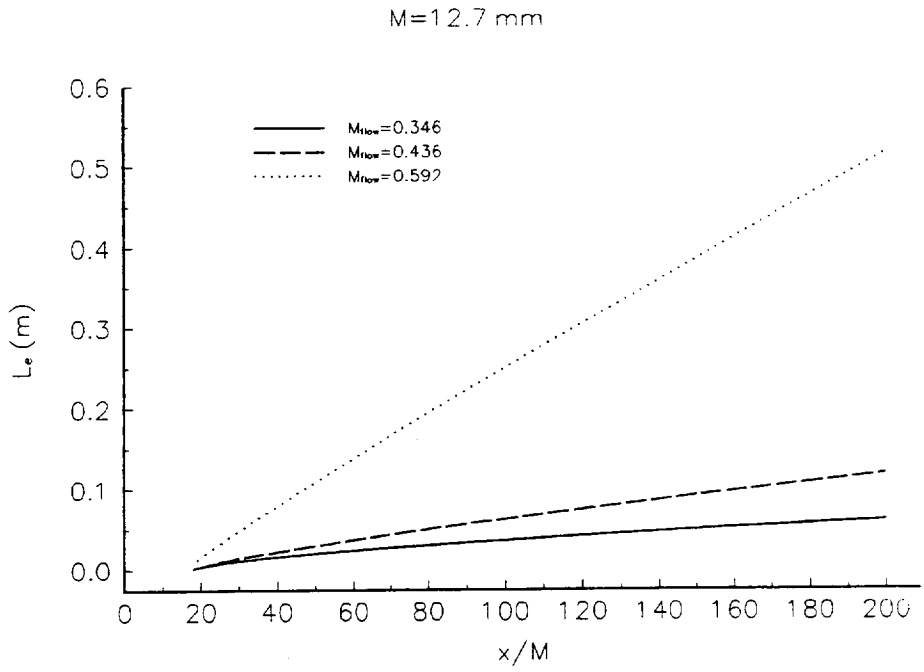

Figure 20: Dissipative length scale for three mean flow Mach numbers.

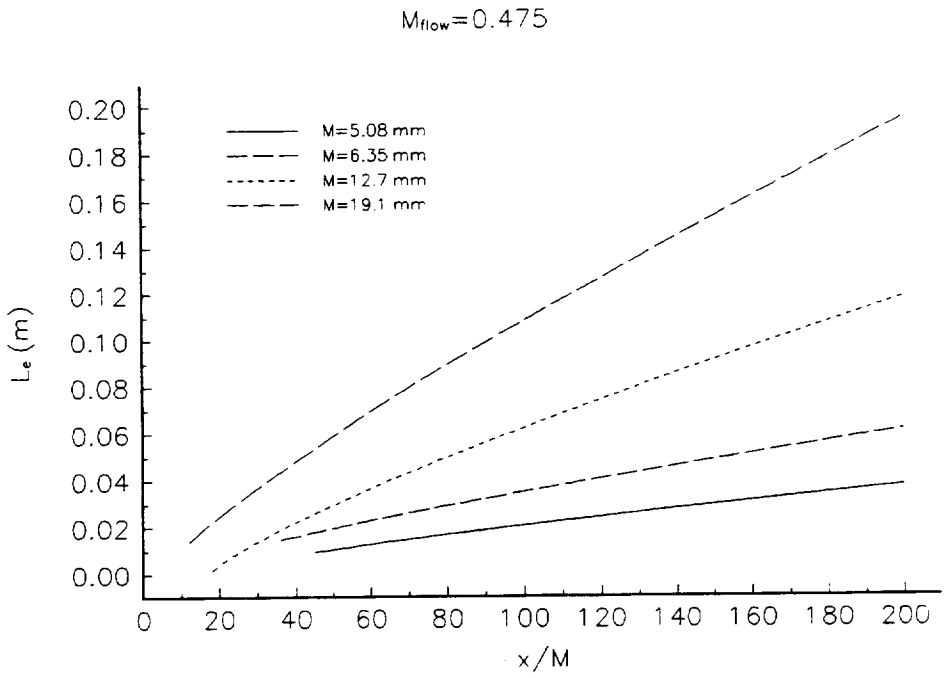

Figure 21: Dissipative length scale for several mesh sizes.

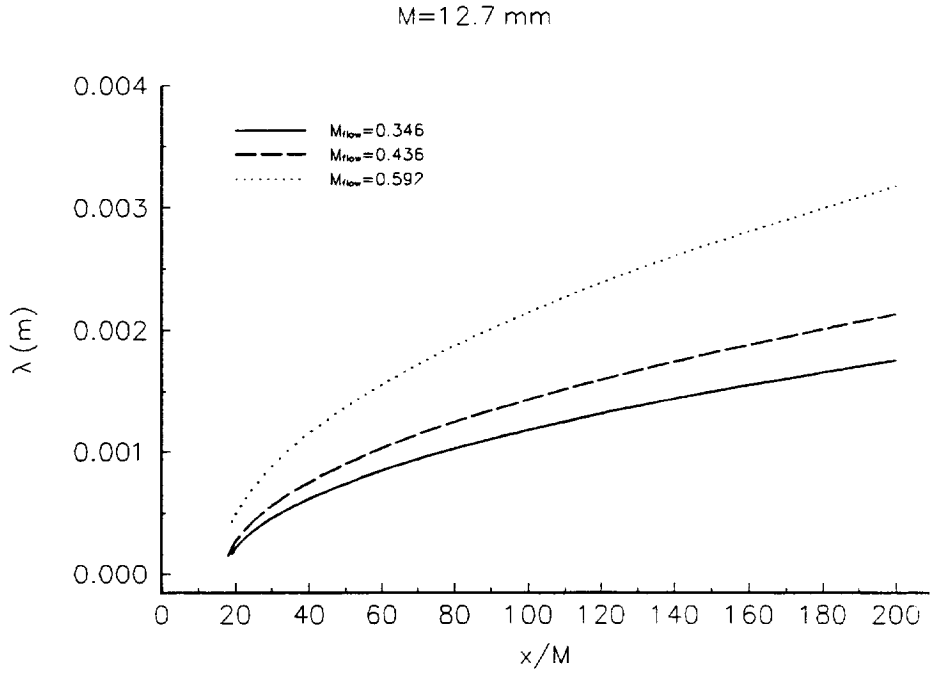

Figure 22: Taylor's microscale for three mean flow Mach numbers.

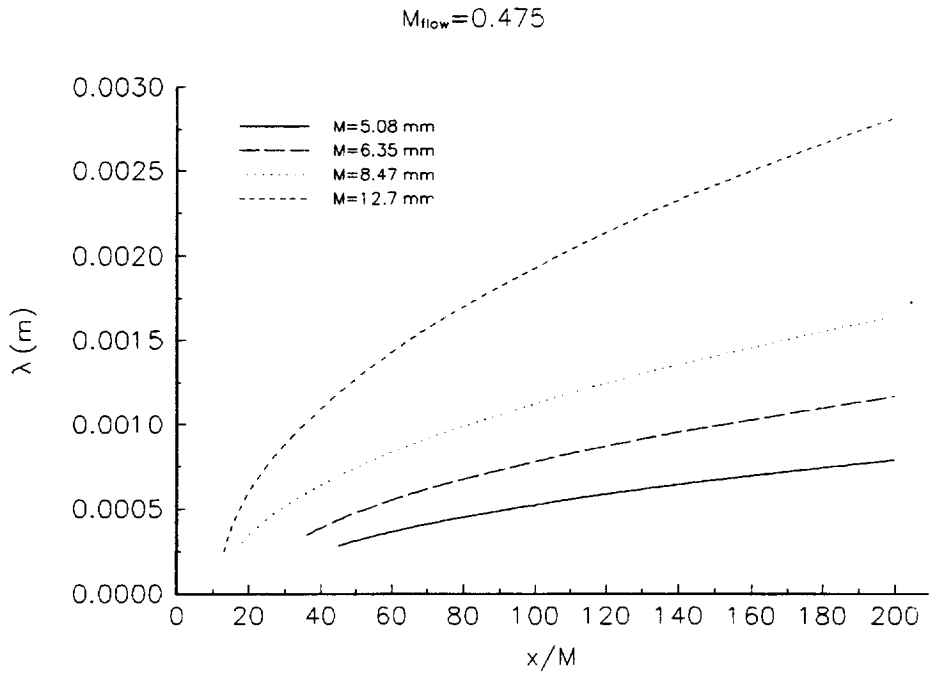

Figure 23: Taylor's microscale for several mesh sizes.

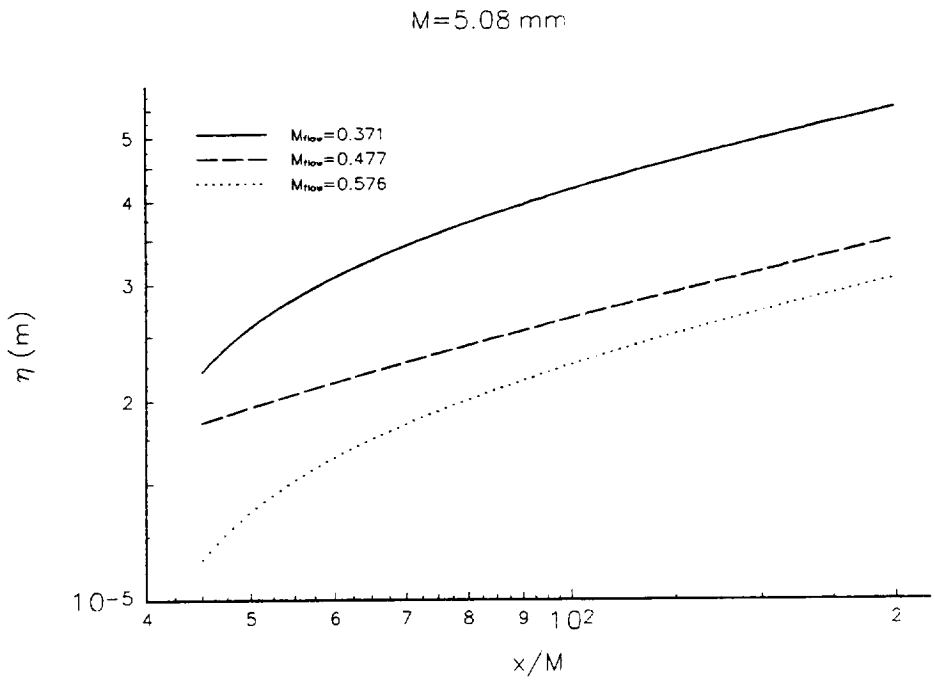

Figure 24: Kolmogorov's length scale for three mean flow Mach numbers.

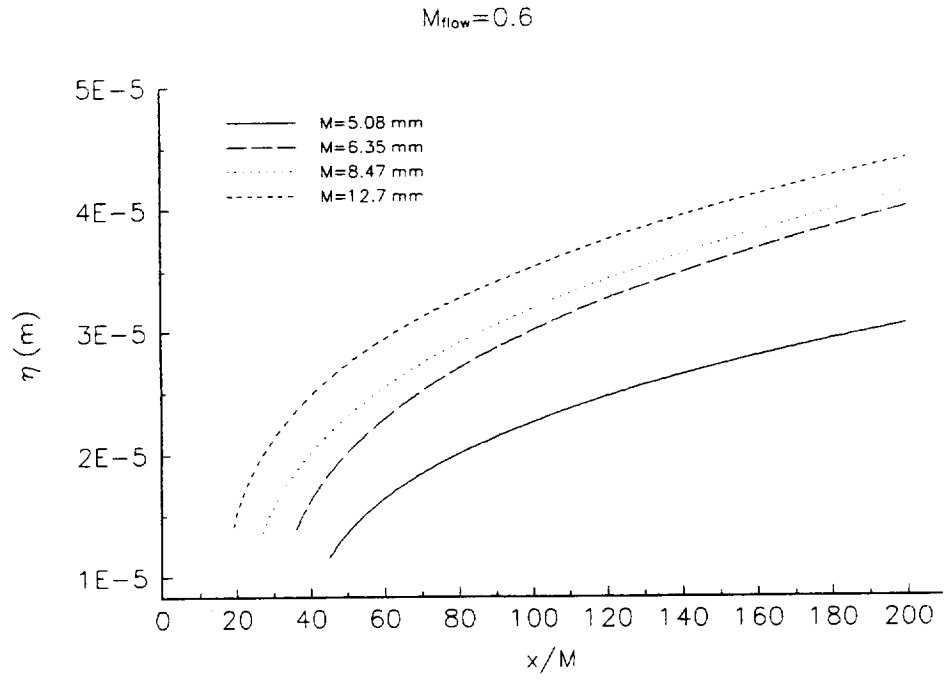

Figure 25: Kolmogorov's length scale for various mesh sizes.

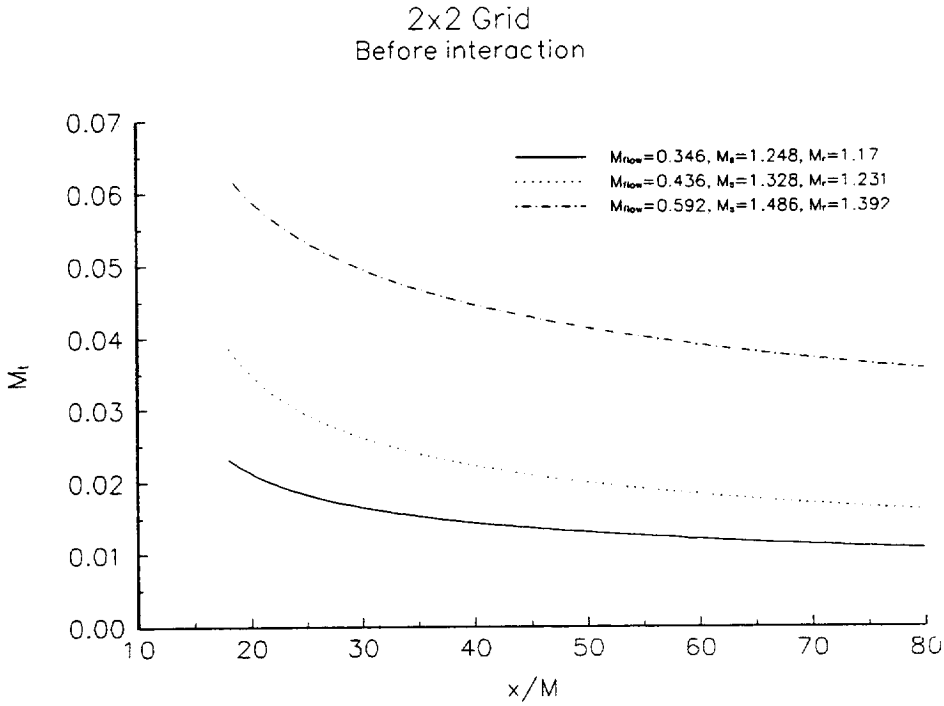

Figure 26a: Mach number fluctuations before interaction with the shock wave.

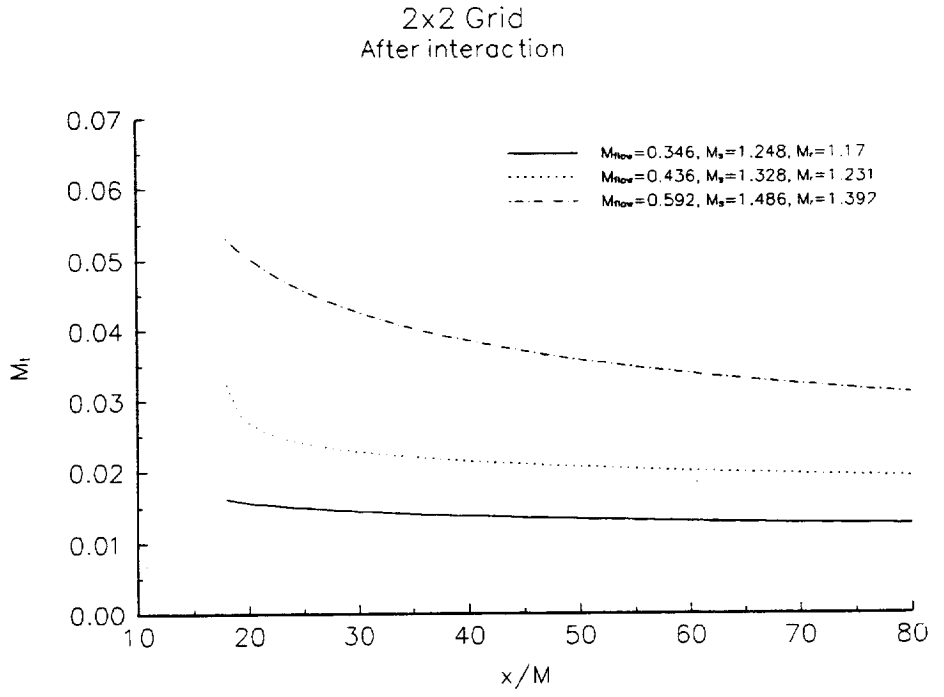

Figure 26b: Mach number fluctuations after interaction with the shock wave.

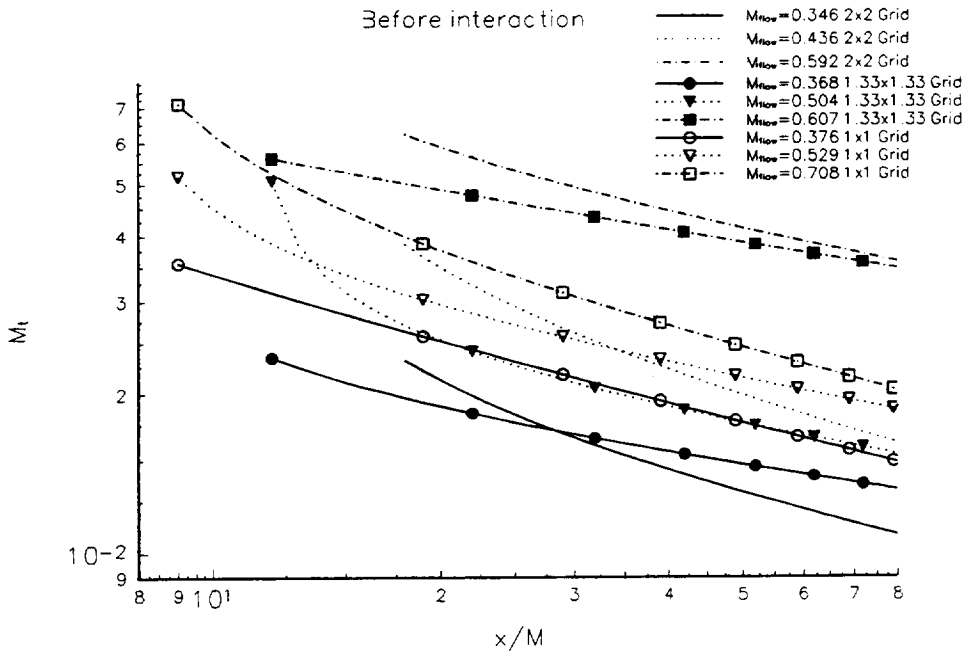

Figure 27a: Mach number fluctuations before interaction with the shock wave.

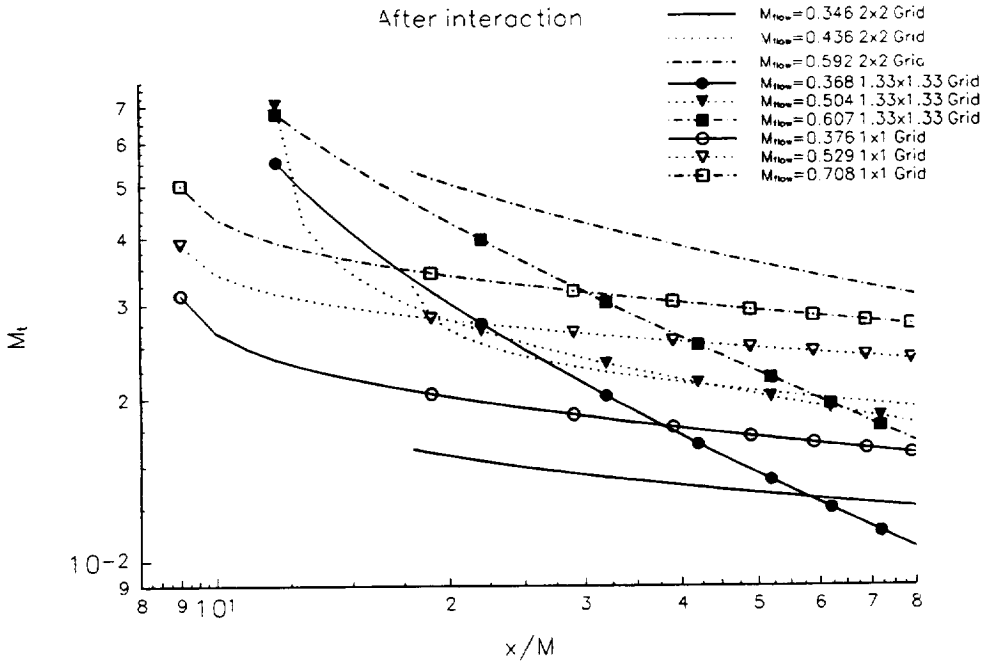

Figure 27b: Mach number fluctuations after interaction with the shock wave.

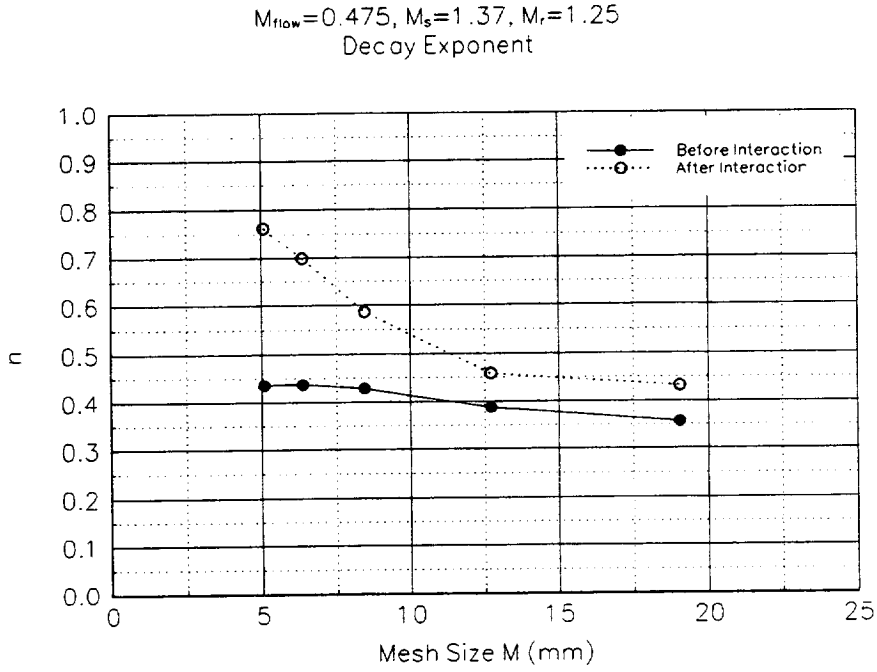

Figure 28: Turbulence decay exponent for various mesh sizes.

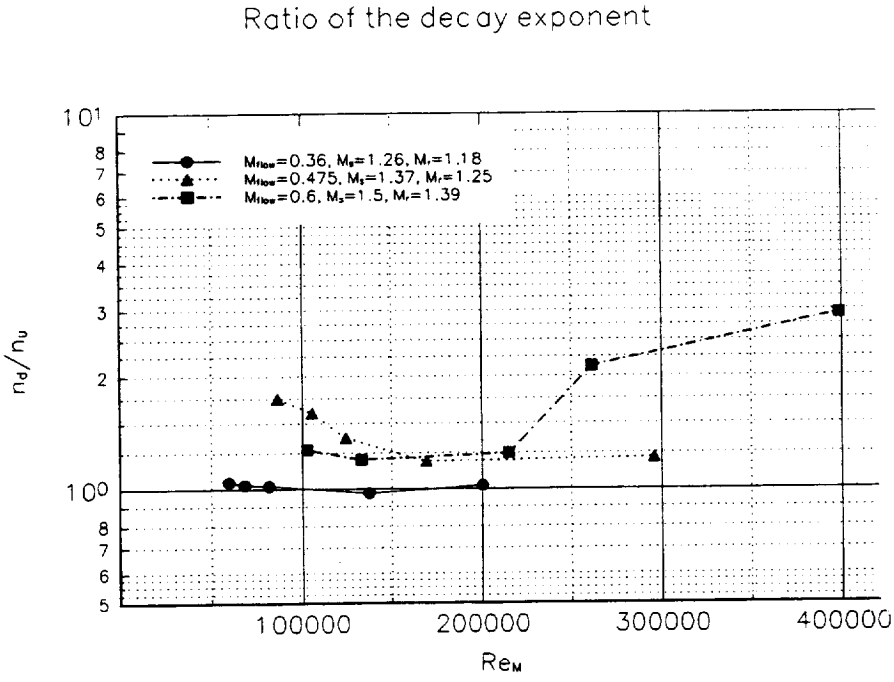

Figure 29: Ratio of the decay exponent for various experiments.

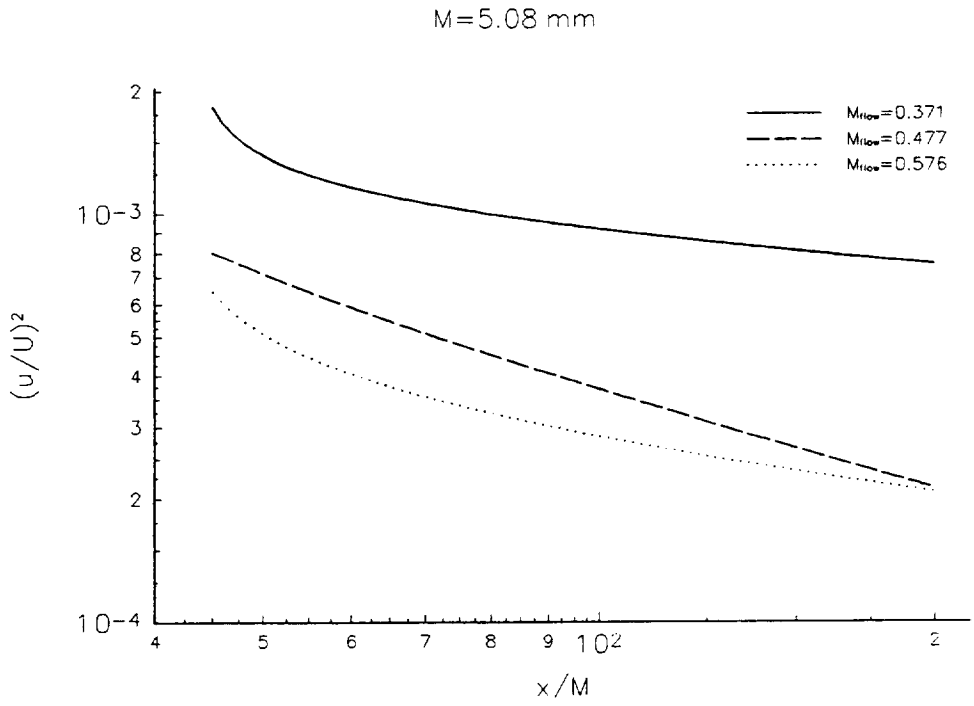

Figure 30: Decay of velocity fluctuations for three Mach numbers at M=5.08 mm.

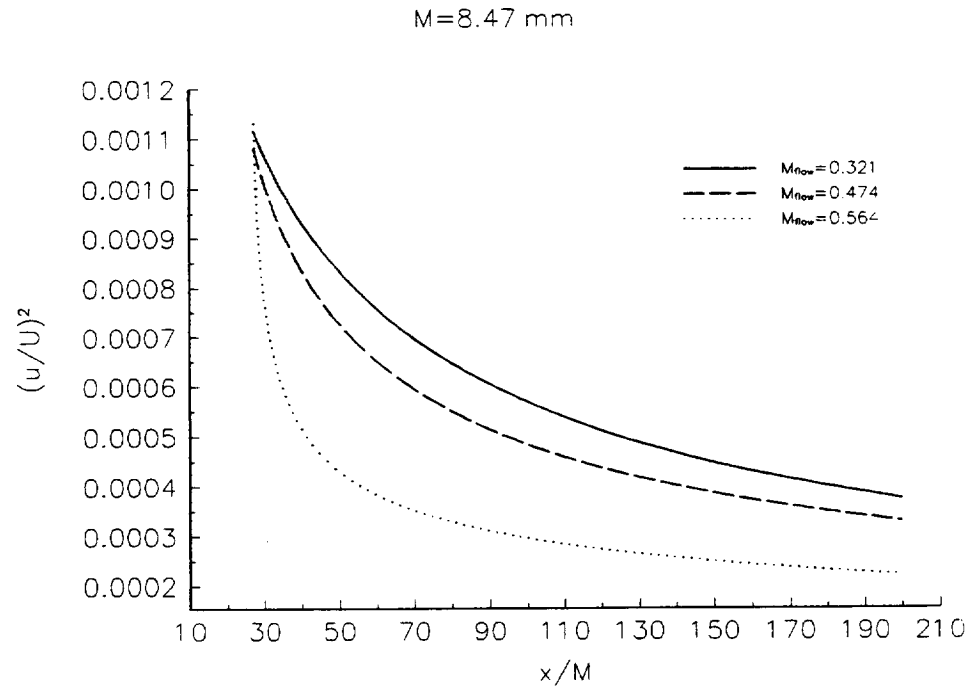

Figure 31: Decay of velocity fluctuations for three Mach numbers at M=8.47 mm.

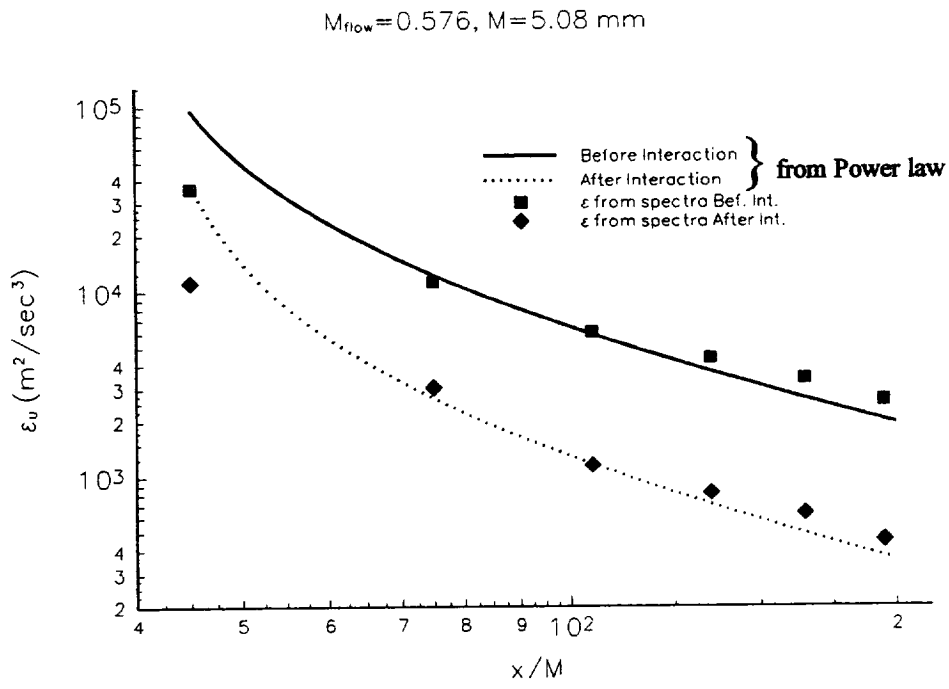

Figure 32: Dissipation rate of kinetic energy before and after interaction at M=5.08mm.

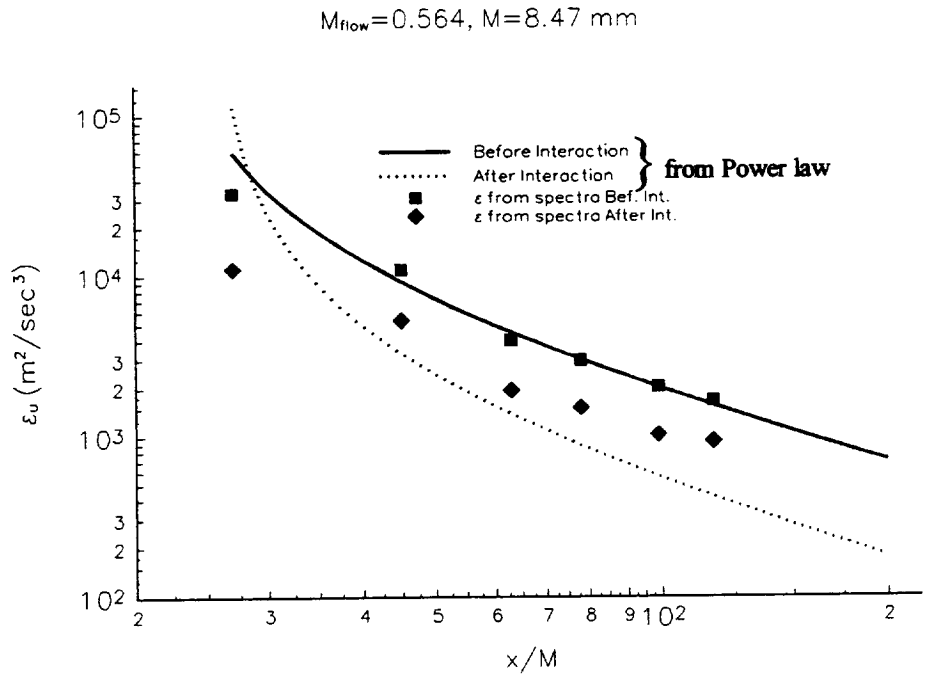

Figure 33: Dissipation rate of kinetic energy before and after interaction at M=8.47mm.

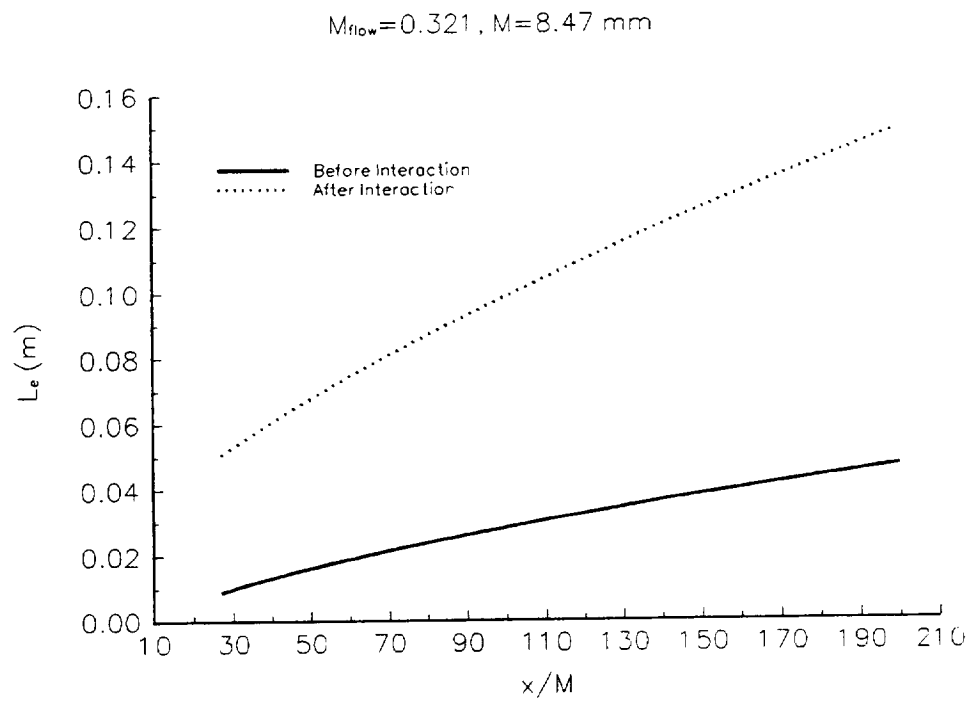

Figure 34: Dissipative length scale before and after interaction at M=8.47 mm.

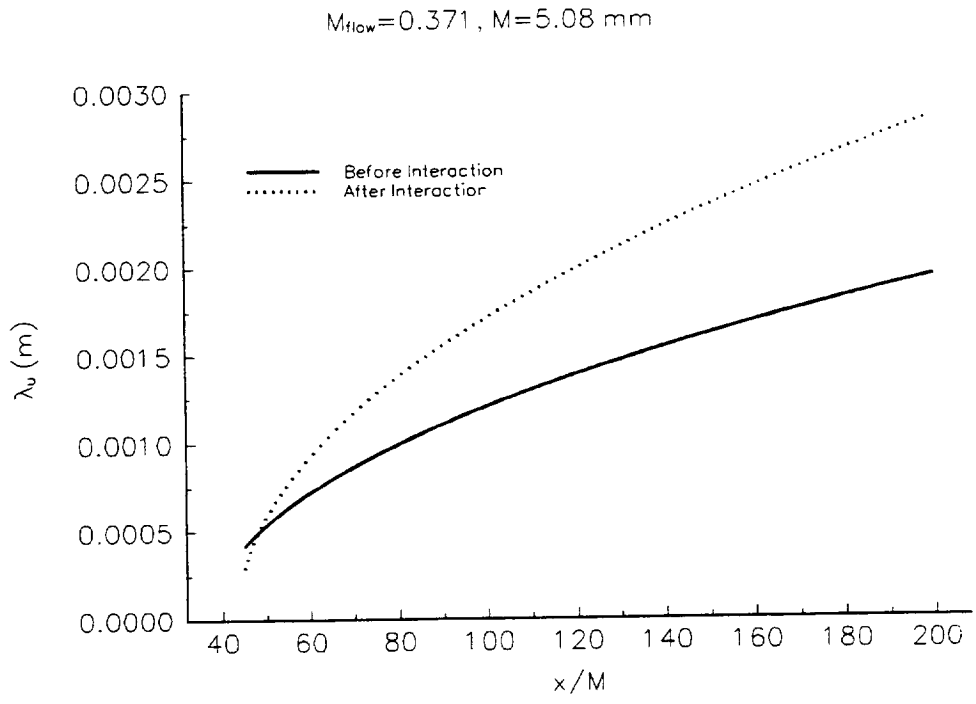

Figure 35: Taylor's microscale before and after interaction at M=5.08 mm.

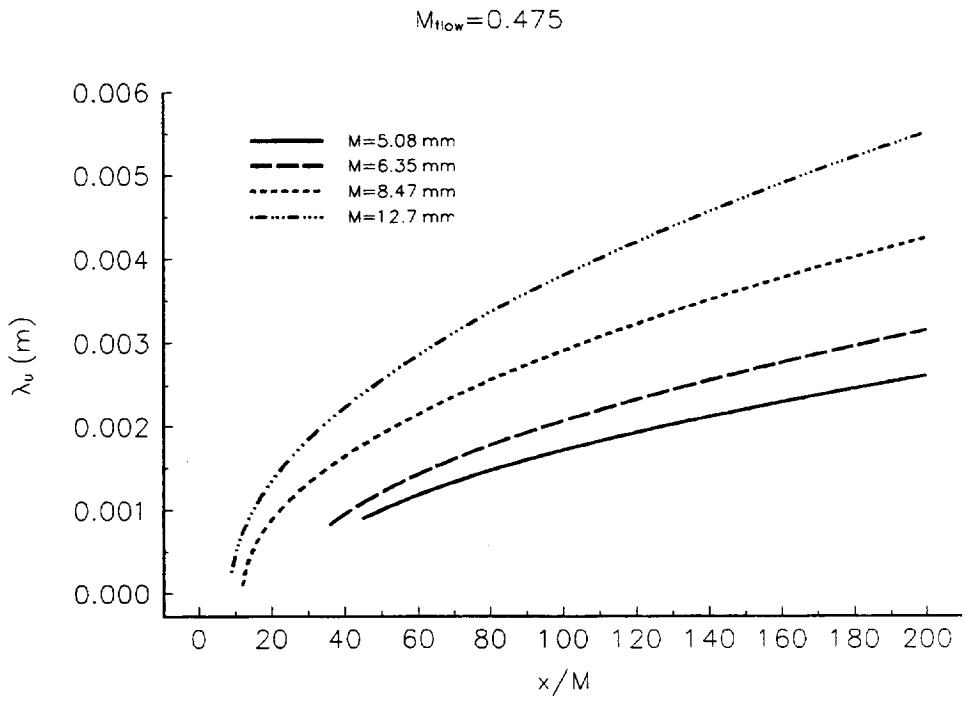

Figure 36: Taylor's microscale at M_{flow}=0.475 for several mesh sizes.

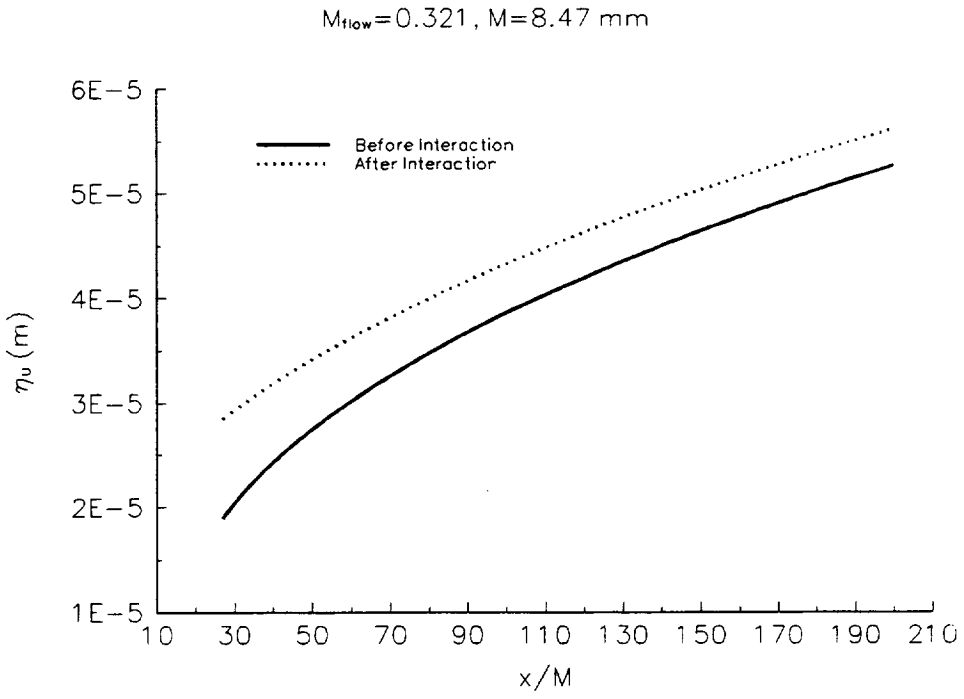

Figure 37: Kolmogorov's length scale before and after interaction at M=8.47 mm.

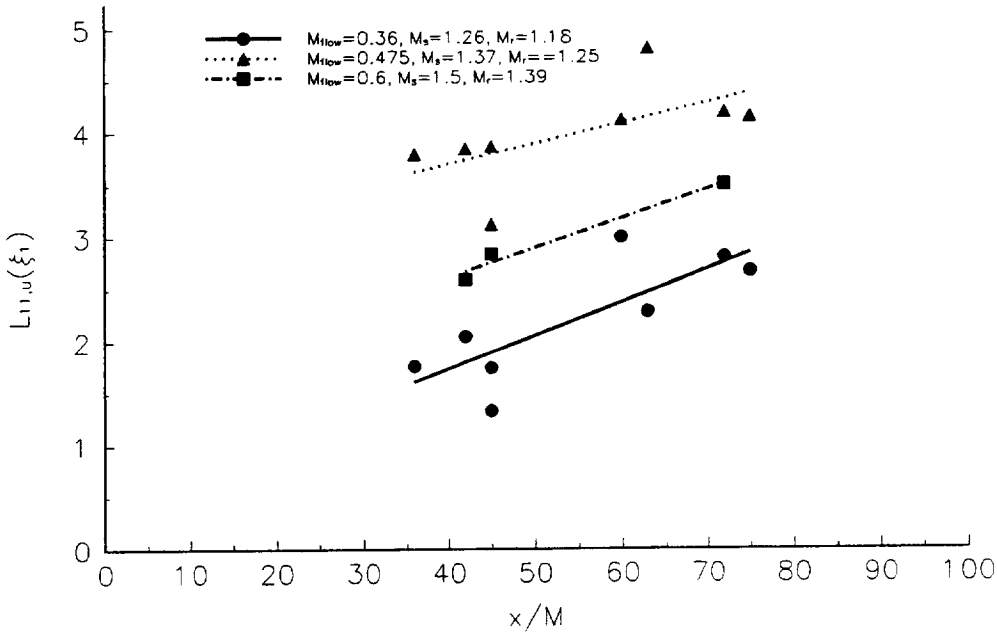

Figure 38: Longitudinal integral length scale for various experiments before interaction with the shock wave.

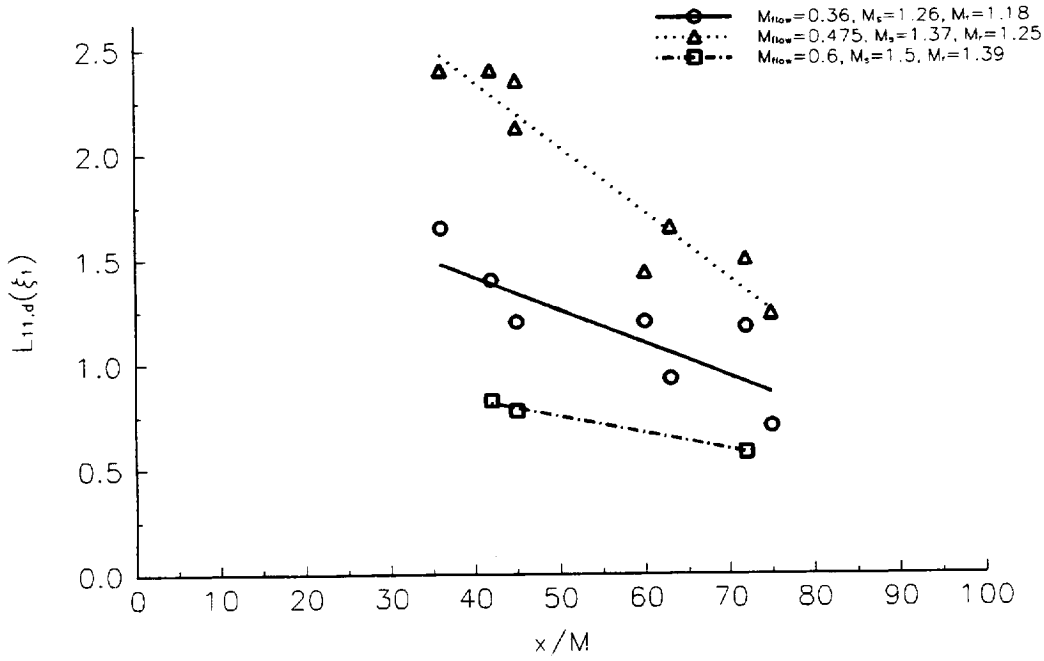

Figure 39: Longitudinal integral length scale for various experiments after interaction with the shock wave.

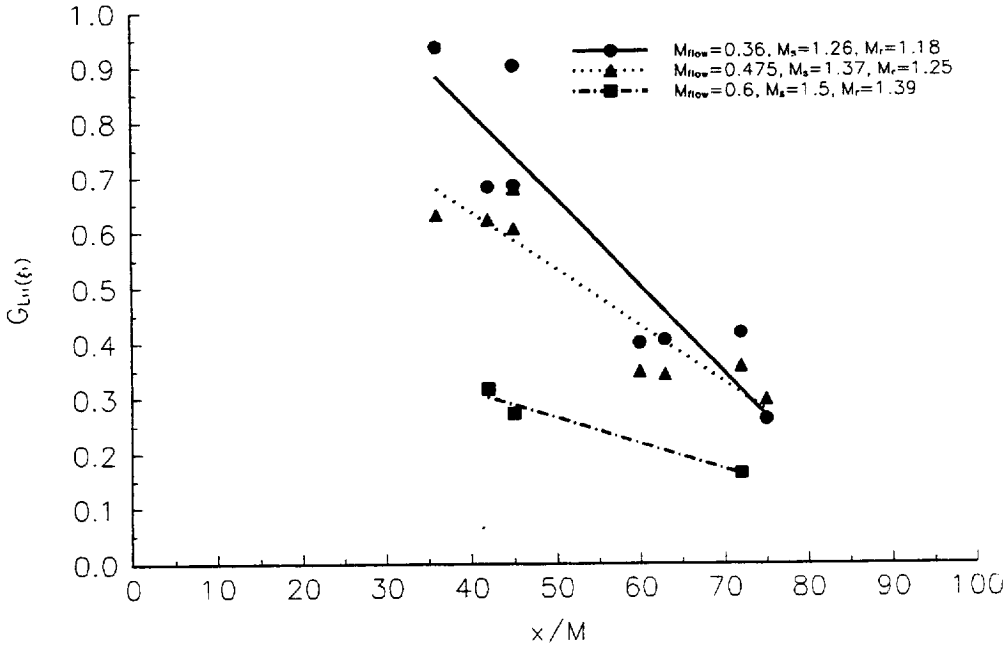

Figure 40: Ratio of the longitudinal integral length scales for various experiments.

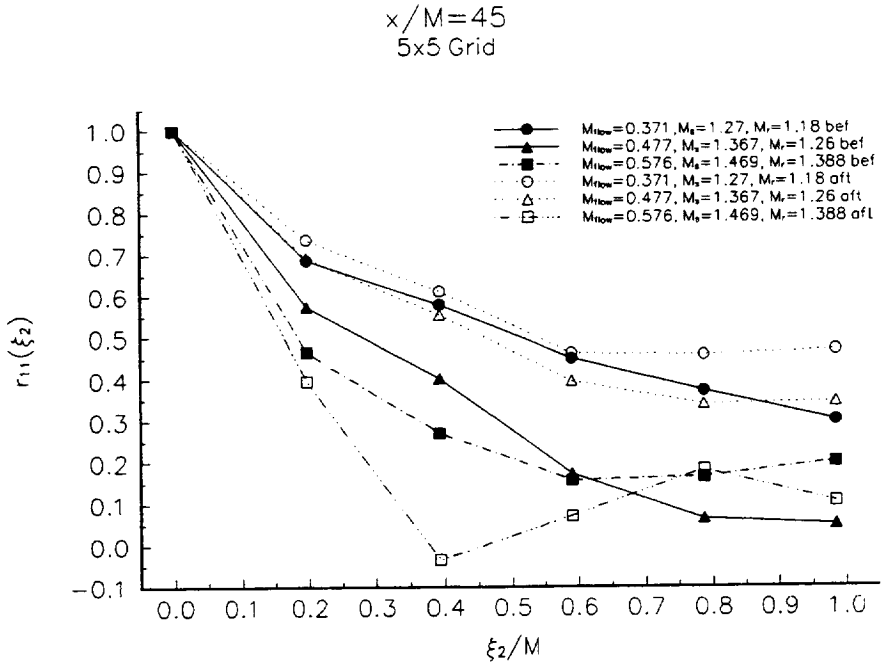

Figure 41: Space correlation in the lateral direction for three different flow cases.

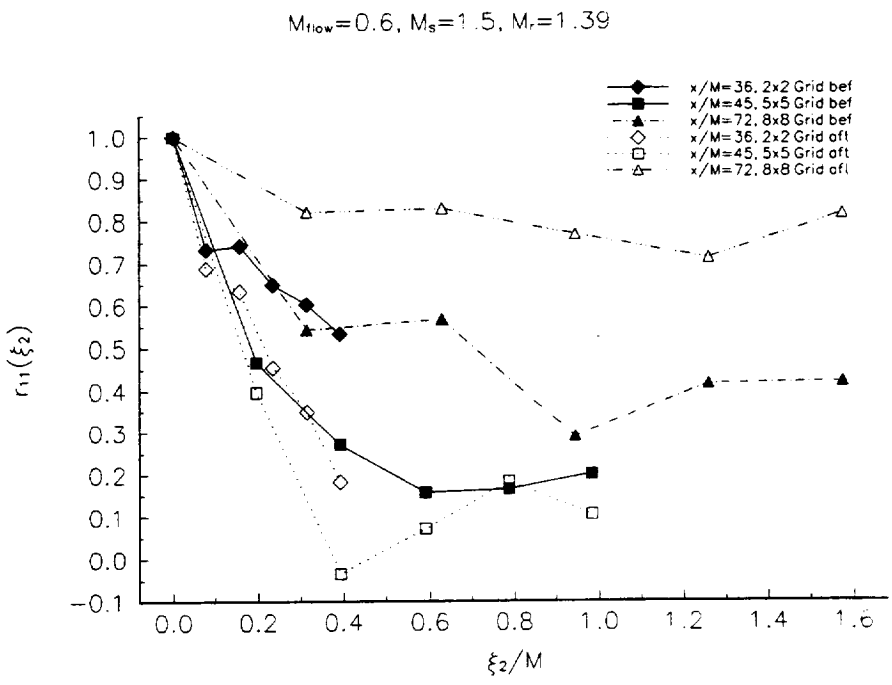

Figure 42: Space correlation in the lateral direction for three different downstream locations.

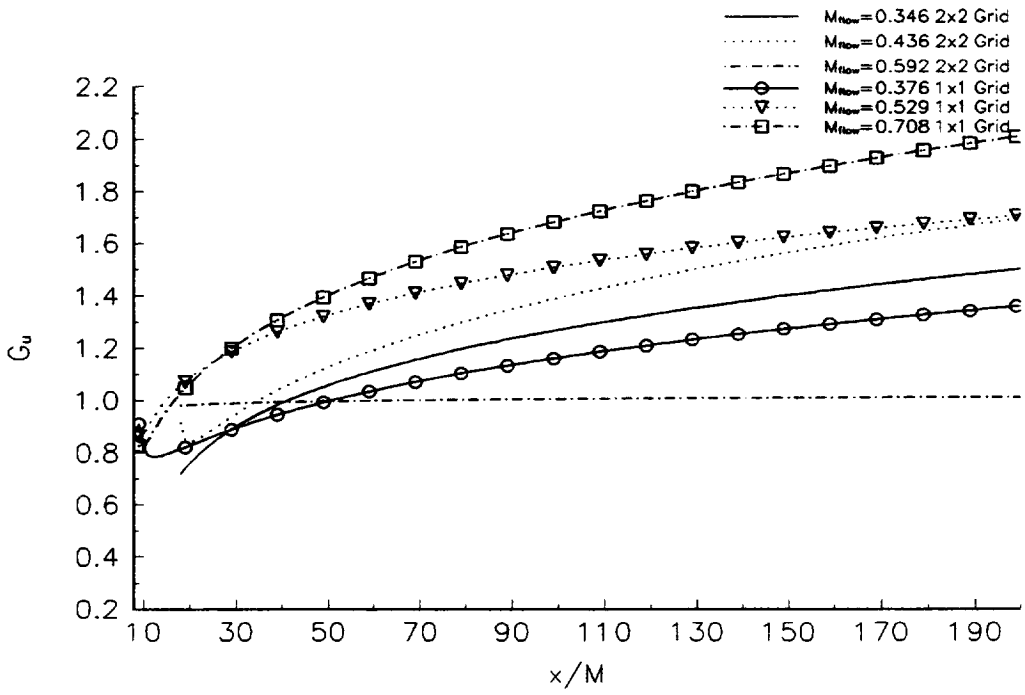

Figure 43: Amplification of velocity fluctuations

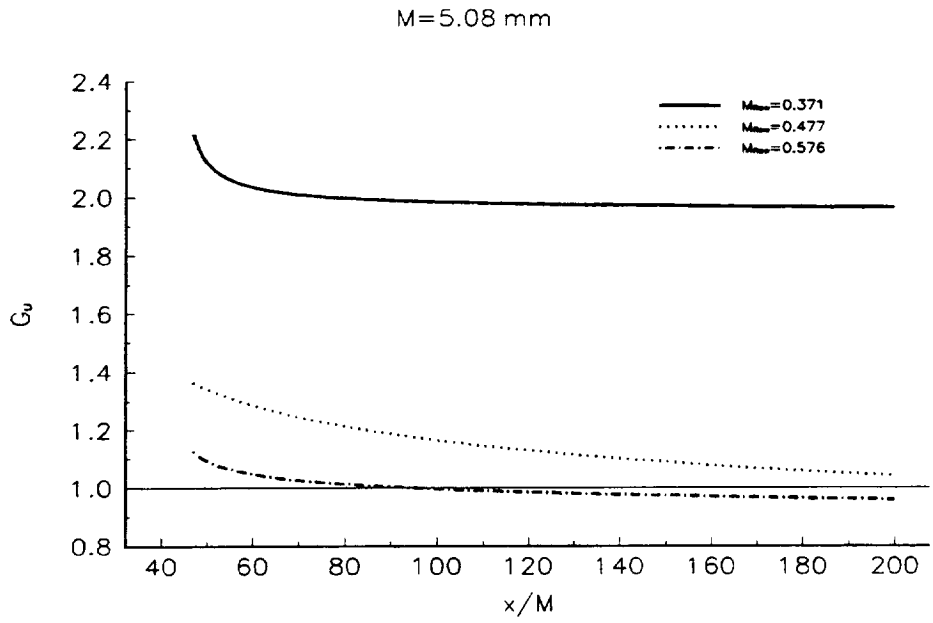

Figure 44: Amplification/Attenuation of velocity fluctuations.

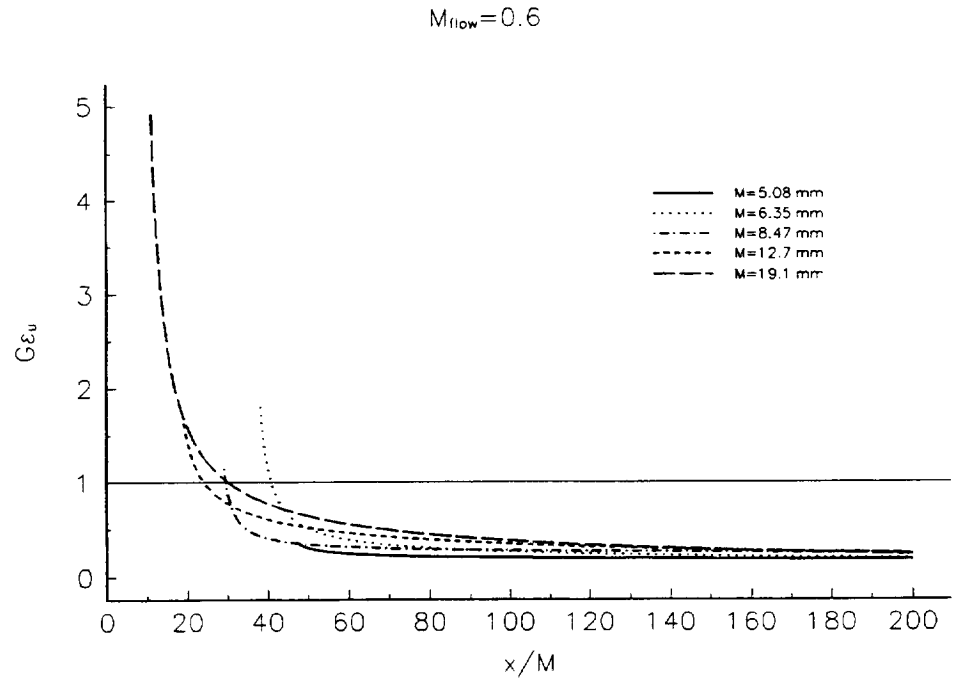

Figure 45: Attenuation of dissipation rate of kinetic energy.

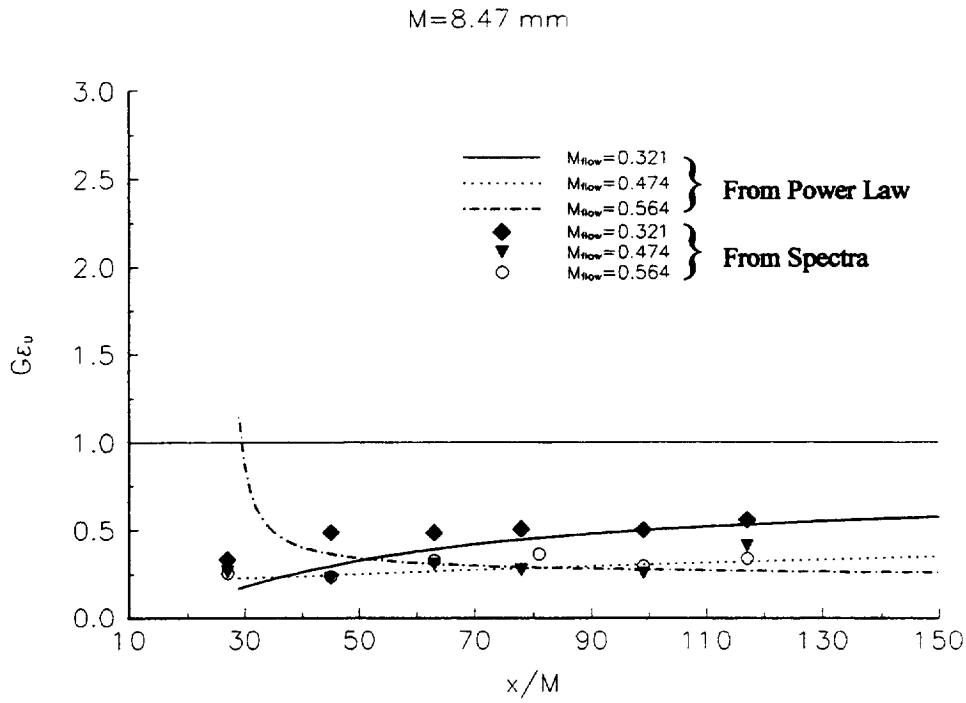

Figure 46: Attenuation of dissipation rate of kinetic energy for three Mach numbers.

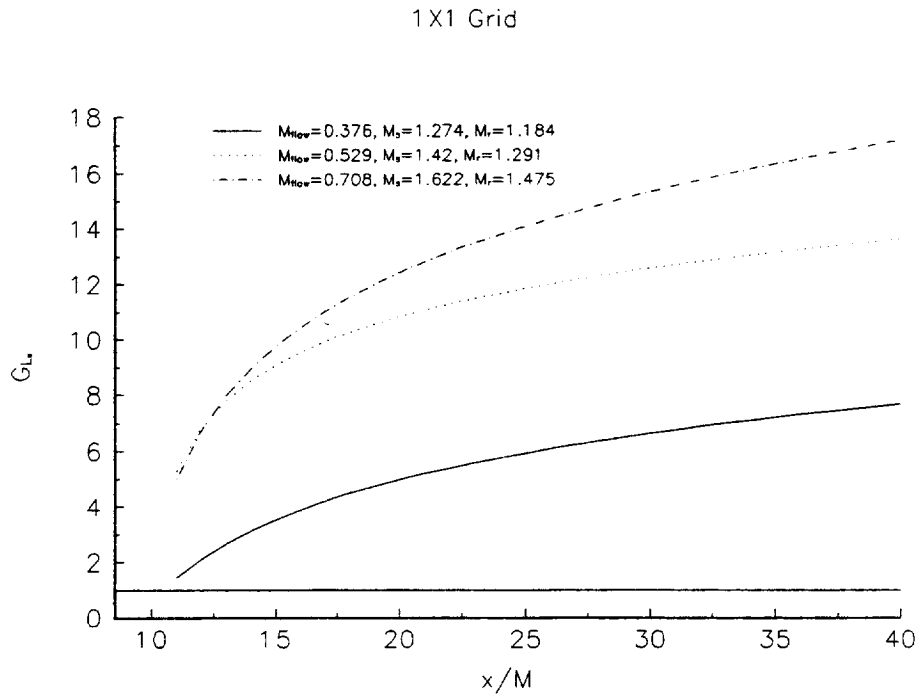

Figure 47: Amplification of the dissipative length scale.

Figure 48: Amplification of the viscous length scale.

Figure 49: Amplification of the Taylor's microscale.

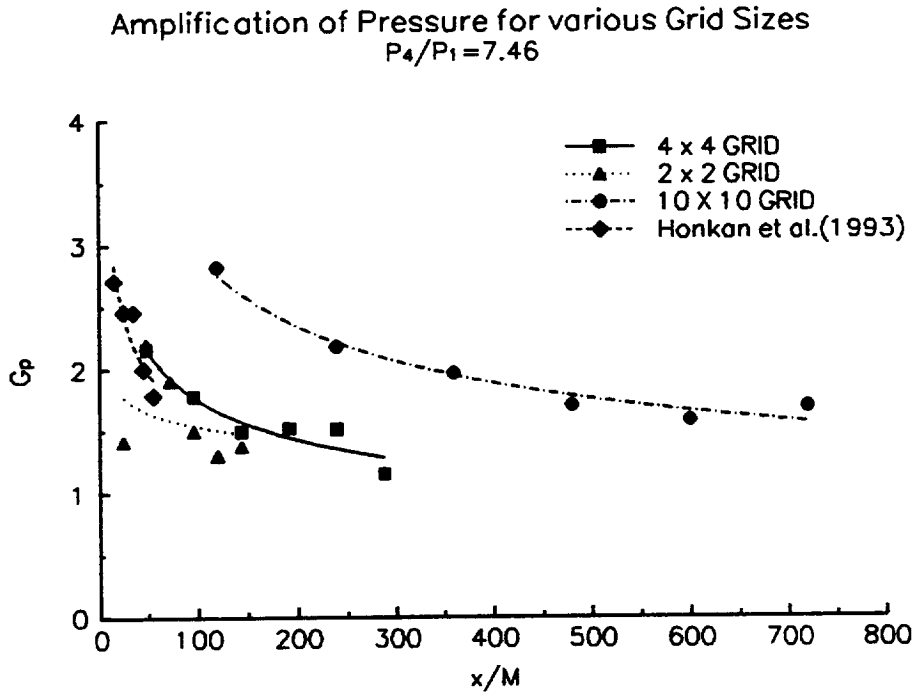

Figure 50: Amplification of wall pressure fluctuations for various grids.

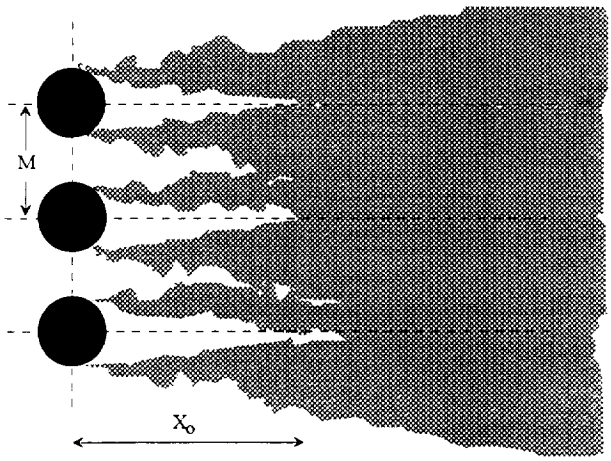

Figure 51a: Incompressible shear layer growth.

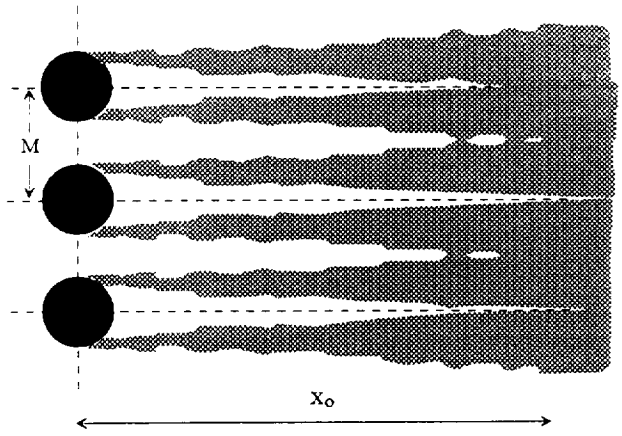

Figure 51b: Compressible shear layer growth.

REPORT DOCUMENTATION PAGE

Form Approved
OMB No. 0704-0188

1. AGENCY USE ONLY *(Leave blank)*	2. REPORT DATE	3. REPORT TYPE AND DATES COVERED
	March 1998	Contractor Report

4. TITLE AND SUBTITLE
Studies of Shock Wave Interactions With Homogeneous and Isotropic Turbulence

5. FUNDING NUMBERS
G NAG1-1590
WU 282-10-01-01

6. AUTHOR(S)
G. Brussels, J. Ague, C. B. Watkins, Y. Andreopoulos

7. PERFORMING ORGANIZATION NAME(S) AND ADDRESS(ES)
The City College of the City University of New York
Department of Mechanical Engineering
New York, NY 10031

8. PERFORMING ORGANIZATION REPORT NUMBER

9. SPONSORING/MONITORING AGENCY NAME(S) AND ADDRESS(ES)
National Aeronautics and Space Administration
Langley Research Center
Hampton, VA 23681-2199

10. SPONSORING/MONITORING AGENCY REPORT NUMBER
NASA/CR-1998-206948

11. SUPPLEMENTARY NOTES
Langley Technical Monitor: Dennis M. Bushnell
Final Report

12a. DISTRIBUTION/AVAILABILITY STATEMENT
Unclassified–Unlimited
Subject Category 34 Distribution: Standard
Availability: NASA CASI (301) 621-0390

12b. DISTRIBUTION CODE

13. ABSTRACT *(Maximum 200 words)*

A nearly homogeneous nearly isotropic compressible turbulent flow interacting with a normal shock wave has been studied experimentally in a large shock tube facility. Spatial resolution of the order of 8 Kolmogorov viscous length scales was achieved in the measurements of turbulence. A variety of turbulence generating grids provide a wide range of turbulence scales. Integral length scales were found to substantially decrease through the interaction with the shock wave in all investigated cases with flow Mach numbers ranging from 0.3 to 0.7 and shock Mach numbers from 1.2 to 1.6. The outcome of the interaction depends strongly on the state of compressibility of the incoming turbulence. The length scales in the lateral direction are amplified at small Mach numbers and attenuated at large Mach numbers. Even at large Mach numbers amplification of lateral length scales has been observed in the case of fine grids. In addition to the interaction with the shock the present work has documented substantial compressibility effects in the incoming homogeneous and isotropic turbulent flow. The decay of Mach number fluctuations was found to follow a power law similar to that describing the decay of incompressible isotropic turbulence. It was found that the decay coefficient and the decay exponent decrease with increasing Mach number while the virtual origin increases with increasing Mach number. A mechanism possibly responsible for these effects appears to be the inherently low growth rate of compressible shear layers emanating from the cylindrical rods of the grid.

14. SUBJECT TERMS	15. NUMBER OF PAGES
Shock interaction; Turbulence amplification; Turbulence scale change	58
	16. PRICE CODE: A04

17. SECURITY CLASSIFICATION OF REPORT	18. SECURITY CLASSIFICATION OF THIS PAGE	19. SECURITY CLASSIFICATION OF ABSTRACT	20. LIMITATION OF ABSTRACT
Unclassified	Unclassified	Unclassified	

NSN 7540-01-280-5500

Standard Form 298 (Rev. 2-89)
Prescribed by ANSI Std. Z39-18
298-102